Pressure dependent mechanical and optoelectronic properties of K_2TeCl_6 vacancy ordered double perovskite: A DFT study

Roll: MS201303
Session: 2020-2021

Thesis submitted to the Department of Physics at
Jashore University of Science and Technology
in partial fulfillment of the requirements
for the degree of Master of Science
in Physics

February, 2024

Abstract

Vacancy ordered double perovskites are outstanding materials for optoelectronic and renewable energy application. In this work, using the full-potential linearized augmented plane wave (FP-LAPW) method based on the density functional theory (DFT) as implemented in the WIEN2k pakage, first principle calculations were performed to investigates the physical properties of vacancy order double perovskites under ambient and uniform pressure. Specifically, the structural, elastic, electronic, and optical properties of K_2TeCl_6 under diverse hydrostatic pressures ranging from 0 to 210 GPa are examined to vendicate the compounds superiority for useful applications. Under ambient pressure, we found a indirect band gap of 2.622 eV for K_2TeCl_6 and which reveals the compound semiconducting nature. Nevertheless, when pressure is increased (0 upto 210 GPa) the band gap narrows. In the pressure range elastic constant, cauchy's pressure, poissons, and pughs ratio show the mechanical stability and ductile behaviour. Likewise, while maintaining mechanical stability, hydrostatic pressure significantly impacts elastic properties. The ductility and anisotropic behaviour of vacancy ordered double perovskite are intensified under applied and uniform pressure. The optical characteristics are analyzed for the incident photon energy range of 0-12 eV by computing dielectric constant, refractive index, optical condutivity, optical reflectivity and absorption coefficients which confirm that our compound is very suitable for device applications in the major parts of the spectrum (visible and ultraviolet). The optical functions are enhanced when pressure is applied, thus vindicating the chosen vacancy order in double perovskites as suitable for various optoelectronic devices operating in the visible and ultraviolet ranges.

Acknowledgements

First and foremost, I would like to express my gratitude to Allah for enabling me to successfully complete this thesis. Following that, I extend my sincere appreciation to my supervisor, Dr. Mohammad Abdur Rashid, for his professional guidance and unwavering support, which has greatly facilitated my learning throughout this thesis. Additionally, I am deeply grateful to the faculty members of the Department of Physics for their valuable suggestions and encouragement provided at various times.

I am also deeply indebted to the members of Quantum Materials Simulation Lab (QMSL) for their constructive suggestions and comments, which significantly contributed to the completion of the thesis within the limited time frame. I extend my thanks to everyone who has been a part of this journey, whether directly or indirectly, contributing to its successful completion. Lastly, I would like to express my heartfelt gratitude to my parents for their unconditional love and prayers, which have always been a source of courage and confidence for me, and a key to my success.

Contents

List of Figures

List of Tables

Pressure dependent mechanical and optoelectronic properties of K_2TeCl_6 vacency ordered double perovskite: A DFT study

Chapter 1

Introduction

In the recent years, the quest for novel compounds for renewable energy conversion with tailored properties continues to drive research towards exploring diverse crystal structures and compositions [1, 2]. Among these intriguing materials, vacancy-ordered double perovskites have emerged as a fascinating class of compounds with promising applications. These materials exhibit a distinctive crystal structure characterized by the precise arrangement of vacancies within the perovskite lattice, offering unique opportunities for tuning their electronic and optical properties [3–5]. In the last few decades, vancy ordered double perovskite compounds have been widely analyzed because of their possible applications in Fourier transform infrared and renewable energy devices [6, 7]. Additionally, due to their better durability with low synthesis cost vancy ordered double perovskites have a common interest for thermoelectric devices [8–10].

Vacancy-ordered double perovskites, characterized by the shared formula A_2BX_6 (with A and B representing metal cations and X representing an anion), have significantly transformed multiple technological sectors, including photovoltaics, photocatalysis, optoelectronics, and the thermoelectric power industry [11–13]. The halide-based vacancy ordered double perovskite material is also an attraction for device use in the visible, infraed as well as ultraviolet regions of the spectrum [14–18].

Introduction

A lot of work has been done on the electronic, optical, as well as thermoelectric characteristics of vacancy ordered double perovskite compounds. For exploring the most efficient, stable, and non-toxic alternatives, the halide (X) based double perovskites (with A_2BX_6 general structural formula) have been investigated. The choice of atoms of varying ionic radii can adjust the structural compositions, which significantly influence the exhibited diverse physical properties. The K_2TiCl_6 and K_2TiBr_6 have the maximum absorption of light from visible to ultraviolet region of spectrum [19]. Solar cells and other optoelectronic applications require them more due to their non-toxic nature and strong structural and thermodynamic stabilities [20–22]. The reported energy band gap 1.6 eV of Cs_2PdBr_6 by theoretical approach is an outstanding breakthrough in solar cell technology [23]. The experimental analysis of Cs_2SnI_6 thin film realize the fascination ability and its possibility for solar cell applications [24]. The structural properties of Te doped Cs_2SnI_6 complex semiconductor has been illustrated by Maughan et al. (2016) and detected the replacement of Sn with Te which reduces the thermoelectric and thermodynamic parameters like electrical conductivity, carrier mobility and carrier concentration [25]. Cai et al.(2017) has analyzed experimentally the electronic structures and effective masses of seven compounds A_2BI_6 where B = Sn, Te, Pt and Pd cations, A = K, Rb and Cs cations. It has been found; the band gap decreases with increasing anion size that leads to structural modification attached with BX_6 octahedra. The E_g $(\Gamma - X)$ 1.47 eV with stable cubic structure is favored the optoelectronic properties [26]. Due to environmental risks and biomedical restrictions, Pb's toxicity prevents its economic utilization [27–30]. Therefore, the demand for Pb-free, highly efficient electronics is enormous. To overcome this problem, different attempts had been performed to replace Pb with inorganic metal cations like tellurium (Te^{4+}) [31], germanium (Ge^{4+}) [32], bismuth (Bi^{3+}) [33], silver (Ag^{+}) etc [34]. Unfortunately, most of them have poor optical efficiency and less stability at ambient conditions. Recently, titanium (Ti) based variant perovskites have been recommended as alternative and promising solution of Pb free perovskites for solar cell applications [35, 36]. In near past, an experiment has been exhibited on cesium titanium bromide Cs_2TiBr_6 for solar with conversion optimum conversion efficiency. Later, Cs_2TiCl/Br_6 for solar

cells [37–39] has undergone a great deal of research. Potential possibilities for solar cells and other optoelectronic applications include Cs_2TiCl/Br_6 due to their excellent stability, non-toxic makeup, visible band gap, and high conversion efficiency [40].

We follow the first-principle calculation method using Density Functional Theory [12, 13] as implemented in WIEN2k code. Density Functional Theory (DFT) is a computational quantum mechanical modeling method used to investigate the electronic structure of many-body systems. DFT is based on the concept of the electron density rather than the wave functions of individual electrons, making it computationally more efficient for studying systems with a large number of electrons [41]. In DFT, the total energy of a system is expressed as a functional of the electron density. The challenge is to find the electron density that minimizes the total energy, subject to the constraints imposed by the external potential from the atomic nuclei. The WIEN2k package is a computer program written in Fortran which performs quantum mechanical calculations on periodic solids. It uses the full-potential (linearized) augmented plane-wave and local-orbitals basis set to solve the Kohn–Sham equations of density functional theory. It was originally developed by Peter Blaha and Karlheinz Schwarz from the Institute of Materials Chemistry of the Vienna University of Technology. The first public release of the code was done in 1990 [42]. It is based on the most accurate scheme for the calculation of the bond structure the full potential energy (linear) augmented plane wave method. In this thesis, we examine the variations in mechanical and optoelectronic properties of K_2TeCl_6 under different pressure conditions, extending up to 210 GPa. A number of physical characteristics, including structural, electronic, and optical properties are frequently explored in detail in order to get a better knowledge of the possible uses of materials. Notably, to properly appreciate a compounds potential for device applications, understanding of elastic constants, moduli, and anisotropy is necessary. The pressure-dependent electronic and optical characteristics are also vital to understand the examined materials viability in optoelectronic applications. Many types of double perovskite oxides compounds were elaborated under ambient pressure and others were synthesized at high pressure, especially,the study of the series Sr_2CrBO_6 compounds based on strontium and chromium where many experimental

and theoretical investigations were reported, due to their structural stability at high temperature, excellent optical properties and high rigidity [43–46].

In this thesis, we begin with the introduction of vacancy ordered double perovskite K_2TeCl_6 materials in the first chapter. In chapter 2 we discuss the basic quantum mechanics which starts with Schrodinger's groundbreaking equation. Chapter 3 contains the theoretical investigation of Density Functional Theory. In this chapter, we discussed the electron density, Thomas-Fermi theory, Hohenberg-Kohn theory, Kohn-Sham equations, Solving the Khon-Sham equation, and the Exchange-correlation potential such as Local density approximation, Hybrid functional approach, Generalized-Gradient Approximation. In Chapter 5, we showcased the outcomes and discussions section of this thesis. In this chapter, our initial focus was on determining the crystal structure. Subsequently, we computed various properties, including the energy band structure, density of states, optical absorption, conductivity, reflectivity, refractivity, real and imaginary dielectric tensor, as well as elastic properties of K_2TeCl_6 under both ambient and uniform pressure conditions. Finally, in chapter 6 we provided a comprehensive summary of this report.

Chapter 2

Basic Quantum Mechnics

The physical features of nature at the size of atoms and subatomic particles are described by the fundamental physics theory known as quantum mechanics. It serves as the theoretical cornerstone for all branches of quantum physics, including quantum information science, quantum technology, quantum field theory, and quantum chemistry. Many features of nature are described by classical physics, the body of ideas that predated the development of quantum mechanics, at a large scale, but it is insufficient to describe them at microscopic scales. The majority of classical physics theories can be approximated by large-scale quantum mechanics [47]. With regard to energy, momentum, angular momentum, and other quantities of a bound system, quantum mechanics differs from classical physics in that these quantities are constrained to discrete values objects have characteristics of both particles and waves and there are restrictions on how precisely a physical quantity can be predicted before being measured, given a complete set of initial conditions.

Erwin Schrödinger utilized de Broglie's connections to describe hypothetical plane waves in his 1926 attempt to characterize the so-called matter waves which led to the most generic version of the famous equation bearing his name, the time-independent Schrödinger equation [48].

$$E\psi(\vec{r}) = \hat{H}\psi(\vec{r}) \tag{2.1}$$

It is often impracticable to use a complete relativistic formulation of the formula; therefore Schrödinger himself postulated a non-relativistic approximation which is nowadays often used, especially in quantum chemistry.

Using the Hamiltonian for a single particle

$$\hat{H} = \hat{T} + \hat{V} = -\frac{\hbar^2}{2m}\vec{\nabla}^2 + V(\vec{r}) \tag{2.2}$$

leads to the (non-relativistic) time-independent single-particle Schrödinger equation

$$E\psi(\vec{r}) = [-\frac{\hbar^2}{2m}\vec{\nabla}^2 + V(\vec{r})]\psi(\vec{r}). \tag{2.3}$$

In this thesis, from now on only non-relativistic cases are considered.

For N particles in three dimensions, the Hamiltonian is

$$\hat{H} = \sum_{i=1}^{N} \frac{{P_i}^2}{2m_i} + V(\vec{r_1}, \vec{r_2}, \ldots, \vec{r}_N) = -\frac{\hbar^2}{2}\sum_{i=1}^{N} \frac{1}{m_i}{\nabla_i}^2 + V(\vec{r_1}, \vec{r_2}, \ldots, \vec{r}_N) \tag{2.4}$$

The corresponding Schrödinger equation reads

$$E\psi(\vec{r_1}, \vec{r_2}, \ldots, \vec{r}_N) = \left[-\frac{\hbar^2}{2}\sum_{i=1}^{N} \frac{1}{m_i}{\nabla_i}^2 + V(\vec{r_1}, \vec{r_2}, \ldots, \vec{r}_N)\right] \psi(\vec{r_1}, \vec{r_2}, \ldots, \vec{r}_N) \tag{2.5}$$

Special cases are the solutions of the time-independent Schrödinger equation, where the Hamiltonian itself has no time-dependency (which implies a time-independent potential $V(\vec{r_1}, \vec{r_2}, \ldots, \vec{r}_N)$, and the solutions therefore describe standing waves which are called stationary states or orbitals). Again, using the many-body Hamiltonian, the Schrödinger equation becomes

$$E\psi(\vec{r_1}, \vec{r_2}, \ldots, \vec{r}_N) = \left[-\frac{\hbar^2}{2}\sum_{i=1}^{N} \frac{1}{m_i}{\nabla_i}^2 + V(\vec{r_1}, \vec{r_2}, \ldots, \vec{r}_N)\right] \psi(\vec{r_1}, \vec{r_2}, \ldots, \vec{r}_N) \tag{2.6}$$

2.1 The wave function

Wave function, in quantum mechanics, variable quantity that mathematically describes the wave characteristics of a particle. The value of the wave function of a particle at a given point of space and time is related to the likelihood of the particle's being there at the time. By analogy with waves such as those of sound, a wave function, designated by the Greek letter Ψ may be thought of as an expression for the amplitude of the particle wave (or de Broglie wave), although for such waves amplitude has no physical significance. The square of the wave function Ψ^2, however, does have physical significance: the probability of finding the particle described by a specific wave function Ψ at a given point and time is proportional to the value of Ψ^2 [49]. The first and most important postulate is that the state of a particle is completely described by its (time-dependent) wave function,i.e.the wave function contains all information about the particle's state. For the sake of simplicity the discussion is restricted to the time-independent wave function. A question always arising with physical quantities is about possible interpretations as well as observations. The Born probability interpretation of the wave function, which is a major principle of the Copenhagen interpretation of quantum mechanics, provides a physical interpretation for the square of the wave function as a probability density [50, 51]

$$|\psi(\vec{r_1}, \vec{r_2}, ..., \vec{r_N})|^2 d\vec{r_1}, d\vec{r_2}...d\vec{r}_N \tag{2.7}$$

Equation(2.9)describes the probability that particles $1, 2, ..N$ are located simultaneously in the corresponding volume element $d\vec{r_1}d\vec{r_2}...d\vec{r}_N$ [52]. It is also necessary to take into account what would happen if two particles' locations were switched. Simple logic dictates that the entire probability density cannot be dependent on such a transaction, i.e.

$$|\psi(\vec{r_1}, \vec{r_2}, \ldots, \vec{r_i}, \vec{r_j}, \ldots \vec{r}_N)|^2 = |\psi(\vec{r_1}, \vec{r_2}, \ldots, \vec{r_j}\vec{r_i}, , \vec{r}_N)|^2 \tag{2.8}$$

The wave function's behavior during a particle exchange has only two possible outcomes. The first is a symmetrical wave function that is unaffected by the exchange. Bosons, or particles with integer or zero spin, correspond to this. The alternative

possibility is an anti-symmetrical wave function, which corresponds to fermions (particles with a half-integer spin), and in which an exchange of two particles results in a sign change [53,54]. In this text only electrons are from interest, which are fermions. The anti-symmetric fermion wave function leads to the Pauli principle,which states that no two electrons can occupy the same state, whereas state means the orbital and spin parts of the wave function [55](the term spin coordinates will be discussed later in more detail). The an-tisymmetry principle can be thought of as Pauli's theoretical concepts in the description of spectra (such as alkaline doublets) being formalized in quantum mechanics [56]. Another consequence of the probability interpretation is the normalization of the wave function. If equation (2.9) describes the probability of finding a particle in a volume element,setting the full range of coordinates as volume element must result in a probability of one, i.e. all particles must be found somewhere in space. This corresponds to the normalization condition for the wave function.

$$\int d\vec{r_1} \int d\vec{r_2} \cdots \int d\vec{r}_N |\psi(\vec{r_1}, \vec{r_2}, \ldots, \vec{r}_N)|^2 = 1 \tag{2.9}$$

Equation (2.11) also reveals the conditions that a wave function must meet in order to be deemed physically acceptable. Wave functions must be square-integratable and continuous over the entire spatial range [57]. Calculating the expectation values of operators using a wave function yields the expectation value of the relevant observable for that wave function, which is another crucial aspect of the wave function [58]. For an obserable $O(\vec{r_1}, \vec{r_2}, \ldots \vec{r}_N)$,this can generally be written as

$$O =< O >= \int d\vec{r_1} \int d\vec{r_2} \cdots \int d\vec{r}_N \psi^*(\vec{r_1}, \vec{r_2}, \ldots, \vec{r}_N) \hat{O} \psi(\vec{r_1}, \vec{r_2}, \ldots, \vec{r}_N) \tag{2.10}$$

Calculating the expectation values of operators using a wave function yields the expectation value of the relevant observable for that wave function, which is another crucial aspect of the wave function,

$$E\psi(\vec{r}) = \left[\frac{\hbar^2}{2m} \vec{\nabla}^2 - \frac{e^2}{4\pi\epsilon_o} . \frac{1}{|\vec{r}|} \right] \psi(\vec{r} \tag{2.11}$$

marks and good starting point. For the sake of simplicity, the so-called atomic units are introduced at this point for subsequent usage. That means the electron mass m_e, the reduced planck constant (Driaction constant)$\hbar$ as well as the vaccum permitivity factor $4\pi\epsilon_o$ are all set to unity [59]. The Schrondinger equation for the single electron simplies to

$$E\psi(\vec{r}) = \left[-\frac{1}{2}\vec{\nabla}^2 - \frac{1}{|\vec{r}|}\right]\psi(\vec{r}) \tag{2.12}$$

This form of the Schrödinger equation is analytically solvable. Although for the description of matter, even atoms, the Schrödinger equation exceeds analytical accessibility soon. Usage of (2.8) allows a construction of a generalized many-body Schrödinger equation for a system composed of N electrons and M nuclei, where external magnetic and electric fields are neglected.

$$E_i\psi_i(\vec{r_1}, \vec{r_2}, \ldots, \vec{r}_N, \vec{R_1}, \vec{R_2}, \ldots, \vec{R_N}) = \hat{H}\psi(\vec{r_1}, \vec{r_2}, \ldots, \vec{r}_N, \vec{R_1}, \vec{R_2}, \ldots, \vec{R}_N) \tag{2.13}$$

Equation (2.15) doesn't seem overly complicated on the first look, but an examination of the corresponding molecular Hamiltonian

$$\hat{H} = -\frac{1}{2}\sum_{i=1}^{N}\vec{\nabla}_i^{\,2} - \frac{1}{2}\sum_{k=1}^{M}\vec{\nabla}_k^{\,2} - \sum_{i=1}^{N}\sum_{k=1}^{M}\frac{Z_k}{r_{ik}} + \sum_{i=1}^{N}\sum_{j>i}^{N}\frac{1}{r_{ij}} + \sum_{k=1}^{M}\sum_{l>k}^{M}\frac{Z_kZ_l}{R_{kl}} \tag{2.14}$$

More generally, it can be written as

$$\hat{H} = \sum_i -\frac{\hbar^2}{2m_e}\vec{\nabla}_i^{\,2} + \sum_I -\frac{\hbar^2}{2m_I}\vec{\nabla}_I^{\,2} + \sum_{iI} -\frac{Z_ie^2}{|\vec{r_i} - \vec{R_I}|} + \frac{1}{2}\sum_{i\neq j}\frac{e^2}{|\vec{r_i} - \vec{r_j}|} + \frac{1}{2}\sum_{I\neq J}\frac{Z_IZ_Je^2}{|\vec{r_i} - \vec{r_j}|} \tag{2.15}$$

reveals the real complexity of the equation. In equation (2.16), M_k repsresents the nuclear mass in atomic units (i.e.in units of the electron mass),Z_k and Z_l represent the atomic numbers,and $\vec{r}_{ij} = |\vec{i} - \vec{j}|, \vec{r}_{ik} = |\vec{i} - \vec{k}|$ and $\vec{R}_{kl} = |\vec{k} - \vec{l}|$ reperesents the distances between the particles (electron-electron nucleus and nucleus-nucleus). A term by term interpretation of the right hand side in (2.16) reveals that the first two terms correspond to the kinetic energies of the electrons and nuclei. The latter three terms denote the potential part of the Hamiltonian in terms of electrostatic

particle-particle interactions. This is reflected by the corresponding signs, where the negative sign denotes an attractive potential between electrons and nuclei, whereas the positive signs denote repulsive potentials between electrons and electrons as well as the nuclei among themselves [60].

2.2 Born-Oppenheimer approximation

The Born-Oppenheimer approximation is one of the basic concepts underlying the description of the quantum states of molecules. This approximation makes it possible to separate the motion of the nuclei and the motion of the electrons. In this discussion nuclear refers to the atomic nuclei as parts of molecules not to the internal structure of the nucleus. The Born-Oppenheimer approximation neglects the motion of the atomic nuclei when describing the electrons in a molecule. Another simplification can be added by taking advantage of the fact that the mass of a proton is around 1800 times greater than the mass of an electron, which is the lowest mass ratio of electron to nucleus (hydrogen atom) and increases even further for heavier atoms. According to the so-called Born-Oppenheimer approximation, the nucleus can be regarded as non-moving, or spatially fixed, in relation to the electrons because of the mass difference. On the timescale of electronic transitions, the core movement can be disregarded, which implies it has no influence on them [50, 61, 62].

As a result, the so-called electronic Hamiltonian replaces the general Hamiltonian

$$\hat{H} = -\frac{1}{2}\sum_{i=1}^{N}\vec{\nabla}_i^{\,2} - \sum_{i=1}^{N}\sum_{k=1}^{M}\frac{Z_k}{r_{ik}} + \sum_{i=1}^{N}\sum_{j>i}^{N}\frac{1}{r_{ij}} \tag{2.16}$$

or in terms of operators

$$H_{el} = \hat{T} + \hat{U} + \hat{V} = \hat{T} + \hat{V_{tot}} \tag{2.17}$$

The electronic Schrödinger equation is of great relevance, especially for quantum chemistry and molecular physics issues. Nevertheless, a quick glance at equations (2.15) to (2.19) shows that there are still a few more important issues to resolve

before a workable solution can be found. Inspection of equations (2.18) and (2.19) shows that the kinetic energy term $\vec{T}$ doesn't depend on the nuclear coordinate R_{kl},or in other words, it is only a function of the electron number. Also the electron-electron repulsion $\vec{U}$ is the same for every system with only Coulomb interactions. Therefore the only part of the electronic Hamiltonian which depends on the atomic respectively molecular system is the external potential V caused by the nucleus-electron repulsion. Subsequently this also means that $\vec{T}$ and $\vec{U}$ the electron number N as input will be therefore be denoted as universal, whereas $\vec{V}$ is system dependent. The expectation value of $\vec{V}$ is also often denoted as the external potential V_{ext},which is consistent as long as there are no external magnetic or electrical fields [58]. As soon as the external potential is known, the next step is the determination of the wave functions ψ_i which contain all possible information about the system. As simple as the sounds, that exact knowledge of the external potentials ,i.e. in similarity to classical mechanics, the largest system which can be solved analytically is a 2-body-system, which corresponds to a hydrogen atom. Using all approximations introduced up to now it is possible to calculate a problem similar to H_2^+a single ionized hydrogen molecule. To get results for larger systems, further approximations have to be made.

2.3 The Hatree-Fock approach

The Coulomb interaction is the root cause of all computing complexity. Maybe there's a way to make this word more computationally tractable, like an effective electron-electron potential $U_{ee}(\vec{r})$. A first guess at such an effective potential in which to study the motion of electrons is that each electron moves in a field produced by a sum over all the other electrons. Analogy with classical physics suggests that the potential corresponding to electron-electron interactions could be

$$U_{ee}(\vec{r}) = \int d\vec{r} \frac{e^2 n(\vec{r'})}{|\vec{r} - \vec{r'}|} \tag{2.18}$$

where n is the number density of electrons

$$n(\vec{r}) = \sum_j |\psi_j(\vec{r})|^2 \tag{2.19}$$

This guess can immediately be inserted into the Schrödinger equation, giving

$$-\frac{\hbar^2}{2m}\vec{\nabla}^2\psi_l + \left[U_{ion}(\vec{r}) + U_{ee}(\vec{r})\right]\psi_l = \epsilon_l\psi_l \tag{2.20}$$

Equation (2.22) is the Hartree equation, which lay behind the first systematic attempts by Hartree (1928) to deduce atomic spectra from first principles [63]. Variational calculus, which is related to the least-action principle of classical mechanics, is a highly helpful tool for determining an appropriate approach to approximating the analytically not accessible solutions of many-body problems. By the use of variational calculus, the ground state wave function which corresponds to the lowest energy of the system can be approached. A useful literature source for the principles of variational calculus has been provided by T.Flieÿbach [64].

Hence, for now only the electronic Schrödinger equation is of interest, therefore in the following sections we set $H \equiv H_{el}$, $E \equiv E_{el}$, and so on. Observables in quantum mechanics are calculated as the expectation values of operators [50, 65]. The energy as observable corresponds to the Hamilton operator,therefore the energy corresponding to a general Hamiltonian can be calculated as

$$E = <\hat{H}>$$

$$= \int d\vec{r_1} \int d\vec{r_2} \cdots \int d\vec{r_N} \psi^*(\vec{r_1}, \vec{r_2}, \ldots, \vec{r_N}) \hat{H} \psi(\vec{r_1}, \vec{r_2}, \ldots, \vec{r_N}) \tag{2.21}$$

The fundamental tenet of the Hartree-Fock technique is that any (normalized) trial wave function other than the actual ground state wave function will always have an energy that is an upper bound, or greater than the actual ground state energy. The energies are equivalent if the trial function turns out to be the intended ground state wave function.

$$E_{trial} \geq E_0 \tag{2.22}$$

with

$$E_{trial} = \int d\vec{r_1} \int d\vec{r_2} \cdots \int d\vec{r}_N \psi^*_{trial}(\vec{r_1}, \vec{r_2}, \ldots, \vec{r}_N) \hat{H} \psi_{trial}(\vec{r_1}, \vec{r_2}, \ldots, \vec{r}_N) \quad (2.23)$$

and

$$E_0 = \int d\vec{r_1} \int d\vec{r_2} \cdots \int d\vec{r}_N \psi^*_0(\vec{r_1}, \vec{r_2}, \ldots, \vec{r}_N) \hat{H} \psi_0(\vec{r_1}, \vec{r_2}, \ldots, \vec{r}_N) \quad (2.24)$$

The expressions above are usually inconvenient to handle. For the sake of a compact notation, in the following the bra-ket notation of Dirac is introduced. For a detailed description of this notation, the reader is referred to the original publication [66]. In this notation, equations (2.24) to (2.26) are expressed as

$$\left\langle \psi_{trial} | \hat{H} | \psi_{trial} \right\rangle = E_{trial} \geq E_0 = \left\langle \psi_0 | \hat{H} | \psi_0 \right\rangle \quad (2.25)$$

Proof :The eigenfunctions psi of the Hamiltonian $\hat{H}$(each corresponding to an energy eigenvalue E_i) form a complete basis set, therefore any normalized trial wave function psi trial can be expressed as linear combination of those eigenfunctions [67].

$$\psi_{trial} = \sum_i \lambda_i \psi_i \quad (2.26)$$

The orthogonality and normalization of the eigenfunctions are taken for granted. It is therefore requested that the trial wave function be normalized, which means

$$\langle \psi_{trial} | \psi_{trial} \rangle = 1 =$$

$$\left\langle \sum_i \lambda_i \psi_i | \sum_j \lambda_j \psi_j \right\rangle = \sum_i \sum_j \lambda_{i^*} \lambda_j \langle \psi_i | \psi_j \rangle = \sum_j |\lambda_j|^2 \quad (2.27)$$

On the other hand,following (2.27) and (2.29)

$$E_{trial} = \left\langle \psi_{trial} | \hat{H} | \psi_{trial} \right\rangle = \left\langle \sum_i \lambda_i \psi_i | \hat{H} | \sum_j \lambda_j \psi_j \right\rangle = \sum_j E_j |\lambda_j|^2 \quad (2.28)$$

In addition to having the smallest eigenvalue ($E_0 \leq E_i$) due to the fact that the

ground state energy E_0 is by definition the lowest energy attainable, it is discovered that

$$E_{trial} = \sum_j E_j |\lambda_j|^2 \geq E_0 \sum_j |\lambda_j|^2 \tag{2.29}$$

similar to equation (2.27) One of the key ideas of density functional theory is the mathematical framework mentioned above, or the laws that give functions numerical values, or functionals. Instead of receiving a numerical input and producing a numerical output, a function receives a function as input and produces a numerical output [68]. Equations (2.23) to (2.31) also include that a search for the minimal energy value while applied on all allowed (physically possible, cf. 2.4 N-electron wave-functions will always provide the ground-state wave function (or wave functions, in case of a degenerate ground state where more than one wave function provides the minimum energy). Expressed in terms of functional calculus, where $\psi\rightarrow$ N addresses all allowed N-electron wave functions, this mean [60].

$$E_0 = \min_{\psi\rightarrow N} E[\psi] = \min_{\psi\rightarrow N} <\psi|\hat{H}|\psi> = \min_{\psi\rightarrow N} <\psi|\hat{T}+\hat{V}+\hat{U}|\psi> \tag{2.30}$$

For N-electron systems this search is, due to the large number of possible wave functions on the one hand and limitations in computational power and time, practically impossible. What is possible is the restriction of the search to a smaller subset of possible wave function, as it is done in the Hartree-Fock approximation. In the Hartree-Fock approach, the search is restricted to approximations of the N- electron wave function by an antisymmetric cf.chapter product of N (normalized) one-electron wave-functions, the so called spin-orbitals $\chi_i(\vec{X}_i)$ [69]. Slater-determinant is the name of a wave function of this kind, and it reads [60, 69].

$$\psi_0 \approx \phi_{SD} = (N!)^{-\frac{1}{2}} = \begin{bmatrix} \chi_1(\vec{x_1}) & \chi_2(\vec{x_1}) & \dots & \chi_N(\vec{x_1}) \\ \chi_1(\vec{x_2}) & \chi_2(\vec{x_2}) & \dots & \chi_N(\vec{x_2}) \\ \vdots & \vdots & \ddots & \vdots \\ \chi_1(\vec{x}_N) & \chi_2(\vec{x}_N) & \dots & \chi_N(\vec{x}_N) \end{bmatrix} \tag{2.31}$$

It's crucial to note that the spin-orbitals $\chi_i(\vec{x_i})$ depend on a spin coordinate introduced by a spin function, $\vec{x_i} = \vec{r_i}, s$ in addition to spatial coordinates. A detailed

discussions of the spin orbitals and their (necessary) properties is omitted in this text, a detailed treatise is provided in the books by Szabo [55] and Holthausen [60]. For atomic calculations, spin orbitals of the type hydrogen and linear combinations of them are utilized as spin orbitals [70]. The ground state energy approximated by a single slater determinant in equation (2.32), going back to the variational principle, becomes

$$E_0 = \min_{\phi_{SD}\to N} E[\phi_{SD}] =$$

$$\min_{\phi_{SD}\to N} \left\langle \phi_{SD}|\hat{H}|\phi_{SD} \right\rangle = \min_{\phi_{SD}\to N} \left\langle \phi_{SD}|\hat{T}+\hat{V}+\hat{U}|\phi_{SD} \right\rangle \tag{2.32}$$

The Hartree-Fock Energy is expressed generally by using the Slater determinant as a trial function.

$$E_{HF} = \left\langle \phi_{SD}|\hat{H}|\phi_{SD} \right\rangle = \left\langle \phi_{SD}|\hat{T}+\hat{V}+\hat{U}|\phi_{SD} \right\rangle \tag{2.33}$$

A thorough derivation of the Hartree-Fock energy's final expression is omitted for the sake of conciseness. It is a simple computation that can be found, for instance, in the book by Schwabl [65]. Three main components make up the Hartree-Fock energy's final representation [60].

$$E_{HF} = \left\langle \phi_{SD}|\hat{H}|\phi_{SD} \right\rangle = \sum_{i}^{N}(i|\hat{h}|i) + \frac{1}{2}\sum_{i}^{N}\sum_{j}^{N}[(ii|jj) - (ij|ji)] \tag{2.34}$$

with

$$\left(i\left|\hat{h}_i\right|i\right) = \int \chi_i^* \left[-\frac{1}{2}\vec{\nabla}_i^{\,2} - \sum_{k=1}^{M}\frac{Z_k}{r_{ik}}\right]\chi_i(\vec{x_i})d\vec{x_i} \tag{2.35}$$

$$(ii|jj) = \int\int |\chi_i(\vec{x_i})|^2 \frac{1}{r_{ij}} |\chi_j(\vec{x_j})|^2 d\vec{x_i}d\vec{x_j} \tag{2.36}$$

$$(ii|jj) = \int\int \chi_i(\vec{x_i})\chi_j^*(\vec{x_j})\frac{1}{r_{ij}}\chi_j(\vec{x_j})\chi_i^*(\vec{x_i})d\vec{x_i}d\vec{x_j} \tag{2.37}$$

The first term denotes the single particle contribution of the Hamiltonian and is associated with the kinetic energy and nucleus-electron interactions, whereas the latter two terms are associated with electron-electron interactions. Coulomb and exchange integral, respectively, are their names [60, 69]. Examination of equations

(2.36) to (2.39) furthermore reveals, that the Hartree-Fock energy can be expressed as a functional of the spin orbitals $E_{HF} = E[\chi_i]$. Thus,variation of the spin orbitals leads to the minimum energy [60]. An important point is that the spin orbitals remain orthonormal during minimization. This restriction is accomplished by the introduction of Lagrangian multipliers χ_i in the resulting equations, which represent the Hartree-Fock equations. For a detailed derivation, the reader is referred to the book by Szabo and Ostlund [60, 64, 69].

At last, one reaches

$$\hat{f}\chi_i = \lambda_i\chi_i \qquad i = 1, 2, 3, \ldots, N \tag{2.38}$$

$$\hat{f}_i = -\frac{1}{2}\vec{\nabla}_i^{\,2} - \sum_{k=1}^{M}\frac{Z_k}{r_{ik}} + \sum_{i}^{N}\left[\hat{j}_j(\vec{x_i}) - \hat{K}_j(\vec{x_i})\right] = \hat{h}_i + \hat{V}^{HF}(i) \tag{2.39}$$

the i^{th} electron's Fock operator. Similar to (2.36) and (2.39), the first two terms are sums over the Coulomb operators $\hat{j}_j$ and the exchange operators K_j with the other j electrons, which together form the Hartree-Fock potential $\hat{V}^{HF}$. These terms represent the kinetic and potential energy due to nucleus-electron interaction, which is collected in the core Hamiltonian $\hat{h}_i$. There, the Hartree-Fock main approximation is visible. A one-electron operator,$\hat{V}^{HF}$, which describes the repulsion on average, replaces the two-electron repulsion operator from the original Hamiltonian [60].

2.4 Limitations and failings of the Hartree-Fock approach

Molecules and atoms can both have an even or an odd number of electrons. The molecule is in a singlet state if the number of electrons is even and they are all positioned in double-occupied spatial orbitals ϕ_i. Closed-shell systems are what these systems are known as. Closed-shell systems are substances with an odd number of electrons as well as substances with a single occupied orbital, i.e., species with a triplet or higher ground state. These two categories of systems relate to two different Hartree-Fock technique approaches. All electrons are assumed to be paired in orbitals when using the restricted HF method (RHF), however this restriction is

completely eliminated when using the unrestricted HF method (UHF). Open-shell systems can also be described using the restricted open-shell HF (ROHF) method, which is more difficult and thus less common than the UHF method but is more realistic since only the single occupied orbitals are excluded [60].

There are also closed-shell systems that demand an open strategy in order to produce quality outcomes. For instance, it is illogical to use a system that places both electrons in the same spatial orbital to describe the dissociation of H_2 (i.e., the behavior at large internuclear distance), because one electron must be positioned at one hydrogen atom. Therefore, while performing HF calculations, the method selection is always of utmost impor tance [69]. The size of the investigated system can also be a limiting factor for calculations. Kohn tates a number of $M = p^5$ with $3 \leq p \leq 10$ parameters for a result with sufficient accuracy in the investigation of the H_2 systems [71]. For a system with $N = 100$ (active) electrons the number of parameters rises to

$$M = p^{3N} = 3^{300} \quad to \quad 3^{300} \approx 10^{150} \quad to \quad 10^{300} \tag{2.40}$$

Equation (2.42) states that the energy minimization would need to be carried out in a space with at least 10^{150} . HF-methods are therefore restricted to systems with a small number of involved electrons ($N \approx 10$). Referring to the exponential factor in (2.42) this limitation is sometimes called exponential wall dimensions, which is considerably above current processing capabilities [71]. The energy determined by HF calculations is usually greater than the precise ground state energy because a multi electron wave function cannot be completely represented by a single Slater determinant. The Hartree-Fock limit is the energy that can be measured with the greatest accuracy using HF methods [60]. The difference between E_{HF} and E_{exact} is called correlation energy and can be denoted as

$$E_{corr}^{HF} = E_{min} - E_{HF} \tag{2.41}$$

Even while E_{corr} is typically modest compared to E_{min}, as in the case of a N_2

molecule,

$$E_{corr}^{HF} = 14.9eV < 0.001.E_{min} \tag{2.42}$$

it can have a huge influence [72]. For instance, the experimental dissociation energy of the N_2 molecule is

$$E_{diss} = 9.9eV < E_{corr} \tag{2.43}$$

It indicates that the correlation energy contributes significantly to relative energies like reaction energies, which are particularly interesting in quantum chemistry [72]. The HF-method's mean field approximation is the primary source of the correlation energy. This implies that one electron flows in the same field as the average of the other electrons, a method that completely ignores the inherent connection of the electron movements. To better grasp what it means, consider how electrons repel one another at close ranges, which is obviously outside the scope of a mean-field technique like the Hartree-Fock method [60].

Chapter 3

Density Functional Theory

Density functional theory has become the method of choice for modeling periodic systems in quantum mechanics over the past 30 years. Recently, quantum chemists have also adopted it, and it is now widely used for modelling the energy surfaces of molecules. In this thesis, we will emphasize the qualities that have made density functional theory so popular and introduce the underlying concepts. We examine functional family families performance and describe current developments in exchange correlation functionals [73]. The electronicThomas-Fermi Theory structure of many body systems, specifically atoms, molecules, and condensed phases, are studied using density functional theory (DFT), a computational quantum mechanical modeling technique. According to this theory, it is possible to ascertain the characteristics of numerous electron systems by employing a function of another function, in this case, the spatial dependency of the electron density. The term density functional theory refers to the usage of electron density functions. The idea put forth in 1965 by Kohn and Sham that the electron kinetic energy should be derived using an additional set of orbitals used to represent the electron density is what led to the development of the contemporary DFT approach [74]. DFT's basic principle is to use a system's particle density rather than its many-body wavefunction to characterize a many-body interacting system. Its importance lies in its ability

to use particle density to reduce the 3N degrees of freedom of the N-body system to only three spatial variables. It is founded on the well-known Hohenberg-Kohn (HK) theory, which asserts that all of a system's features may be seen as distinct functionals of its ground state density.ogether with the Born-Oppenheimer (BO) approximation and Kohn-Sham (KS) ansatz, practical accurate DFT calculations have been made possible via approximations for the so called exchange-correlation (XC) potential, which describes the effects of the Pauli principle and the Coulomb potential beyond a pure electrostatic interaction of the electrons. Since it is impossible to calculate the exact (XC) potential (by solving the many-body problem exactly), a common approximation is the so called local density approximation (LDA) which locally substitutes the XC energy density of an inhomogeneous system by that of a homogeneous electron gas evaluated at the local density. In many cases the results of DFT calculations for condensed matter systems agreed quite satisfactorily with experimental data, especially with better approximations for the XC energy functional since the 1990s. Also, the computational costs were relatively low compared to traditional ways which were based on the complicated many-electron wave function, such as Hartree-Fock theory and its descendants. Despite the improvements in DFT, there are still difficulties in using DFT to properly describe intermolecular interactions; charge transfer excitations; transition states, global potential energy surfaces and some other strongly correlated systems; and in calculations of the band gap of some semiconductors [75].

3.1 A new base variable - the electron density

A general statement regarding the calculation of observables has been given in the section 2.1 about the wave function. This section discusses a quantity calculated in a very similar manner. As the primary variable in density functional theory, the electron density (for N electrons) is defined as [52, 60].

$$n(\vec{r}) = N \sum_{s_1} \int d\vec{x_2} \ldots \int d\vec{x}_N \psi^*(\vec{x_1}, \vec{x_2}, \ldots, \vec{x}_N)\psi(\vec{x_1}, \vec{x_2}, \ldots, \vec{x}_N) \tag{3.1}$$

What has to be mentioned is that the notation in (3.1) considers a wave function dependent on spin and spatial coordinates. In detail, the integral in the equation gives the probability that a particular electron with arbitrary spin is found in the volume element$d\vec{r_1}$. Due to the fact that the electrons are indistinguishable, N times the integral gives the probability that any electron is found there. The other electrons represented by the wave function $\psi(\vec{x_1}, x_2, \ldots, \vec{x_N})$ have arbitrary spin and spatial coordinates [52]. If additionally the spin coordinates are neglected, the electron density can even be expressed as measurable observable only dependent on spatial coordinates [71, 76].

$$n(\vec{r}) = N \int d\vec{r_2} \ldots \int d\vec{r}_N \psi^*(\vec{r_1}, \vec{r_2}, \ldots, \vec{r}_N)\psi(\vec{r_1}, \vec{r_2}, \ldots, \vec{r}_N) \tag{3.2}$$

which, for example, X-ray diffraction can measure [60]. Before presenting an approach using the electron density as variable, it has to be ensured that it truly contains all necessary informations about the system. In detail that means it has to contain information about the electron number N as well asthe external potential characterized by $\hat{V}$ [60]. The total number of electrons can be obtained by integration the electron density over the spatial variables [60].

$$N = \int d\vec{r} n(\vec{r}) \tag{3.3}$$

What needs to be demonstrated is that the electron density also uniquely characterizes the external potential, where uniquely denotes up to an additive constant.

3.2 Thomas-Fermi Theory

One of the earliest tractable schemes for solving the many-electron problem was proposed by Thomas and Fermi [77, 78]. In this model, the electron density $n(r)$ is the central variable rather than the wave function, and the total energy of a system is written as a functional $E_{TF}[n(r)]$ where square brackets are used to enclose the argument of the functional, which in this case is the density. The Thomas-Fermi

energy functional is composed of three terms,

$$E_{TF}[n(\vec{r})] = A_k \int n(\vec{r})^{5/3} dr + \int n(\vec{r}) V_{ext} dr + \frac{1}{2} \int \int \frac{n(\vec{r}) n(\vec{r'})}{|\vec{r} - \vec{r'}|} \tag{3.4}$$

The first term is the electronic kinetic energy associated with a system of non-interacting electrons in a homogeneous electron gas. This form is obtained by integrating the kinetic energy density of a homogeneous electron gas t_0 $[n(r)]$ [79].

$$T^{TF}[n(\vec{r})] = \int t_0[n(\vec{r}] d\vec{r} \tag{3.5}$$

where $t_0[n(\vec{r}]$ is obtained by summing all of the free-electron energy states $\varepsilon = \frac{K^2}{2}$ up to the Fermi wave vector $K_F = [3\pi^2 n(\vec{r})]^{\frac{1}{3}}$

$$t_0[n(r)] = \frac{2}{2\pi^3} \int \frac{k^2}{2} n_k dk = \frac{1}{2\pi^3} \int_0^k F k^4 dk \tag{3.6}$$

n_k is the density of allowed states in reciprocal-space. This leads to the form given in (3.7) with coefficient $A_k = \frac{3}{10}(3\pi^2)^{\frac{2}{3}}$. The power-law dependence on the density can also be stablished on dimensional grounds. The second term is the classical electrostatic energy of attraction between the nuclei and the electrons, where $U_{ext}(\vec{r})$ is the static Coulomb potential arising from the nuclei,

$$U_{ext}(\vec{r}) = -\sum_{j=1}^{M} \frac{z_j}{|\vec{r} - \vec{R_j}|} \tag{3.7}$$

Finally, the third term in (3.6) represents the electron-electron interactions of the system, and in this case is approximated by the classical Coulomb repulsion between electrons, known as the Hartree energy.

To obtain the ground state density and energy of a system, the Thomas-Fermi equation (3.8) must be minimized subject to the constraint that the number of electrons is conserved. This type of constrained minimization problem, which occurs frequently within many-body methods, can be performed using the technique of Lagrange multipliers. In general terms, them minimization of a functional $F[f]$,

subject to the constraint $C[f]$, leads to the following stationary condition

$$\delta(F[f] - \mu C[f]) = 0 \tag{3.8}$$

where $\mu$is a constant known as the Lagrange multiplier. Minimizing (3.11) leads to the solution of the corresponding Euler equation,

$$\frac{\delta F[f]}{\delta f} - \mu \frac{\delta C[f]}{\delta f} \tag{3.9}$$

Applying this method to (3.5) leads to the stationary condition,

$$\delta E_{TF}[n(\vec{r})] - (\int n(\vec{r}) - \int n(\vec{r}) d\vec{r} - N) \tag{3.10}$$

which yields the so-called Thomas-Fermi equations

that can be solved directly to obtain the ground state density, Thomas-Fermi theory suffers from many deficiencies, probably the most serious defect is that it does not predict bonding between atoms [80–82], so molecules and solids cannot form in this theory. The main source of error comes from approximating the kinetic energy in such a crude way. The kinetic energy represents a substantial portion of the total energy of a system and so even small errors prove disastrous. Another shortcoming is the over-simplified description of the electron-electron interactions, which are treated classically and so do not take account of quantum phenomenon such as the exchange interaction.

3.3 Hohenberg-Kohn theorems

According to the basic lemma of Hohenberg-Kohn [83], not only is $n(\vec{r})$ a functional of $v(\vec{r})$, but also $n(\vec{r})$ is up to a constant that is solely defined by $n(\vec{r})$ [60, 71, 76].Since the original publication of Hohenberg and Kohn deals with an electron gas,the Hamiltonian is resembled by the electronic Hamilton operator introduced in equation (2.18) $\hat{H}_{el} = \hat{T} + \hat{V} + \hat{U}$with the one difference that the non-universal contribution $\hat{V}$in this case represents a general external potential (which in caseof

the electronic Hamilton approximated by Born-Oppenheimer contains a nuclear field contribution) [58, 60, 76].

The discussion in this thesis is limited to non-degenerate ground states, following Hohenberg and Kohn's original strategy and their proof by reductio ad absurdum [76]. This restriction nevertheless doesn't affect the presented proof for the second theorem and can be lifted as well for the first theorem [84, 85].

the energy of the system can be denoted as

$$E = \langle\psi|\hat{H}|\psi\rangle = \langle\psi|\hat{T}+\hat{V}+\hat{U}|\psi\rangle = \int v(\vec{r})n(\vec{r})d\vec{r} + \langle\psi|\hat{T}+\hat{U}|\psi\rangle \tag{3.11}$$

This will be applied to demonstrate Hohenberg and Kohn's initial theorem.

3.3.1 Theorem 1

The external potential $v(\vec{r})$ is a functional of the electron density $n(\vec{r})$ and, up to an unimportant constant, uniquely determined by it [76].

Proof : It is assumed that there exist two external potentials $v(\vec{r})$ and $v'(\vec{r})$which differ by more than just a trivial constant. Furthermore, the assumption is made, that both potentials give rise to the same electron density $n(\vec{r})$. Clearly, arising from the nature of $\hat{V}n$that case there have to be two different Hamiltonians $\hat{H}$ and $\hat{H}'$. Furthermore ψ and ψ' have to be different, since they fulfill different Schrödinger equations. Finally also the energies E and E' associated with the particular wave function differ [71, 86].

Now the two wave functions ψ and ψ' are used as trial functions assuming the other wave function is the ground state wave function. Then the expressions

$$E_0' = \langle\psi'|\hat{H}'|\psi'\rangle \quad < \quad \langle\psi'|\hat{H}'|\psi'\rangle =$$

$$\langle\psi|\hat{H}+\hat{V}'-\hat{V}|\psi\rangle = \langle\psi|\hat{H}|\psi\rangle + \langle\psi|\hat{V}'-\hat{V}|\psi\rangle \tag{3.12}$$

and

$$E_0 = \langle\psi|\hat{H}|\psi\rangle < \langle\psi'|\hat{H}|\psi'\rangle$$

$$\langle\psi'|\hat{H}' + \hat{V} - \hat{V}'|\psi'\rangle = \langle\psi'|\hat{H}'|\psi'\rangle + \langle\psi'|\hat{V} - \hat{V}'|\psi'\rangle \tag{3.13}$$

are obtained. By the use of (3.11), this can be rewritten as

$$E_0' < E_0 + \int [v'(\vec{r}) - v(\vec{r})]n(\vec{r})d\vec{r} \tag{3.14}$$

and

$$E_0 < E_0' + \int [v(\vec{r}) - v'\vec{r})]n(\vec{r})d\vec{r} \tag{3.15}$$

By summation of (3.14) and (3.15) the inequality

$$E_0' + E_0 < E_0 + E_0' \tag{3.16}$$

is obtained, which represents an inconsistency and therefore provides by reduction to absurdity the proof $v(\vec{r})$ is truly a unique functional of $n(\vec{r})$. The first Hohenberg-Kohn theorem can also be written in another form which is sometimes called the strong form of the Hohenberg-Kohn theorem [87]. Here $\Delta v(\vec{r})$ and $\Delta n(\vec{r})$ correspond to the change in potential and electron density respectively:

$$\int \Delta v(\vec{r})\Delta n(\vec{r}) < 0 \tag{3.17}$$

Whereas equation (3.17) can be derived from the original proof [48] it can also be derived perturbatively. The importance of this proof lies in the fact, that it not only implies the first Hohenberg Kohn theorem (if $\Delta v(\vec{r}) \neq 0$ clearly also must not vanish) but also provides an assertion about the signs of $\Delta v(\vec{r})$ and $\Delta n(\vec{r})$ i.e. a (mostly) positive potentialrequires a (mostly) negative electron density $\Delta n(\vec{r})$ to ensure the negativity of the integral in (3.17) [87].

From the first Hohenberg Kohn theorem it is obvious that also the ground state

wave function is a unique functional of the ground state electron density

$$\psi_0(\vec{r_1}, \vec{r_2}, \ldots, \vec{r_N}) = \psi[n_0(\vec{r})] \tag{3.18}$$

Furthermore, recalling (2.12), the ground state expectation value of any observable is a functional of $n_0(\vec{r})$ too, i.e.

$$O_0 = O[n_0(\vec{r})] = \langle \psi[n_0(\vec{r})] | O | \psi[n_0(\vec{r})] \rangle \tag{3.19}$$

Among these observables is the ground state energy, the expectation value of the Hamiltonian, which is of great importance. Recalling equation (3.11), the ground state energy corresponding to an potential $v(\vec{r})$ can be denoted as

$$E_{v,0} = E_v[n_0(\vec{r})] = \left\langle \psi[n_0(\vec{r})] | \hat{H} | \psi[n_0(\vec{r})] \right\rangle$$

$$\int v(\vec{r}) n_0(\vec{r}) d\vec{r} + \left\langle \psi[n_0(\vec{r})] | \hat{T} + \hat{U} | \psi[n_0(\vec{r})] \right\rangle \tag{3.20}$$

To obtain a more convenient handling of equation (3.13), the Hohenberg-Kohn functional $F_{HK}[n(\vec{r})]$ and subsequently, the energy functional $E_v[n(\vec{r})]$ are defined [76].

$$F_{HK}[n(\vec{r})] \equiv \left\langle \psi[n_0(\vec{r})] | \hat{T} + \hat{U} | \psi[n_0(\vec{r})] \right\rangle \tag{3.21}$$

$$E_v[n(\vec{r})] \equiv \int v(\vec{r}) n_0(\vec{r}) d\vec{r} + F_{HK}[n(\vec{r})] \tag{3.22}$$

In similarity to the terminology introduced in the section about the HartreeFock method, the Hohenberg-Kohn functional represents the system independent or universal part. Equation (3.20) furthermore leads to another crucial finding of the original paper by Hohenberg and Kohn, which is often addressed as the second theorem of Hohenberg and Kohn [76].

3.3.2 Theorem 2

Using variational calculus, the ground state energy can be calculated from the electron density. The exact ground state density is therefore the electron density, which

offers the smallest amount of ground state energy. The principle of energy variation is stated in the second Hohenberg-Khon theorem. It implyes that for any trial density which is not ground state density in a condition $n'(\vec{r}) \geqslant 0$ and $\int n'(\vec{r})dr = N$. That is

$$E_0 \leqslant E_v[n'] \tag{3.23}$$

Where $E_v[n']$ is the energy functional of next equation (3.25) Originally this second theorem has been proved by variation calculus, [76] the proof provided subsequently is a different one, namely the so called constrained-search approach, introduced by Levy and Lieb [88,89].and subsequently thoroughly examined in the books by Parr, Yang as well as Kryachko and Ludena [90,91]. Since the wave function is a unique functional of the electron density, every trial wave function ψ' corresponding to a trial density $n'(\vec{r})$ following equation (3.2). According to the Rayleigh-Ritz principle, the ground state energy is obtained as

$$E_{v,0} = \min_{\psi'} \left\langle \psi' | \hat{H} | \psi' \right\rangle \tag{3.24}$$

Proof : The minimizing can, in theory, be done in two steps.In the first step, a trial electron density $n'(\vec{r})$ is fixed. The class of trial functions corresponding to that electron density is then denoted by $\psi'^{\alpha}_{n'}$ [71],Then, the constrained energy minimum is defined as

$$E_v[n'(\vec{r})] = \min_{\alpha} \left\langle \psi'^{\alpha}_{n'} | \hat{H} | \psi'^{\alpha}_{n'} \right\rangle = \int v(\vec{r}) n'(\vec{r}) d\vec{r} + F[n'(\vec{r})] \tag{3.25}$$

In that notation, $F[n'(\vec{r})]$ is the functional

$$F[n'(\vec{r})] \equiv \min_{\alpha} \left\langle \psi'^{\alpha}_{n'} | \hat{T} + \hat{U} | \psi'^{\alpha}_{n'} \right\rangle \tag{3.26}$$

which is clearly related to the Hohenberg-Kohn functional in (3.20). What is important to notice at this point is that the universal functional $F[n'(\vec{r})]$ requires no explicit knowledge of $v(\vec{r})$.

In the second step, equation (3.12) is minimized over all trial densities $n'(\vec{r})$:

$$E_{v,0} = \min_{n'(\vec{r})} E_v[n'(\vec{r})] = \min_{n'(\vec{r})} \left\{ \int v(\vec{r}) n'(\vec{r}) d\vec{r} + F[n'(\vec{r})] \right\} \tag{3.27}$$

Now, assuming $F[n'(\vec{r})]$ is the real ground state density, the energy in (3.27) is obtained for a non-degenerate ground state. Additionally, the restriction to non-degenerate ground states is finally lifted by the constrained search methodology. Only one of the wave functions linked to the energy of the degenerate ground state is found if a ground state density corresponding to a number of wave functions is chosen [60]. In summary, it has been demonstrated that the electron density can be used as a base variable inside the framework of density functional theory, which is precise mathematically.Recapitulating, it has been shown that density functional theory provides a clear and mathematical exact framework for the use of the electron density as base variable. Nevertheless, nothing of what has been derived is of practical use. Or in other words, the Hohenberg-Kohn theorems,as important as they are, do not provide any help for the calculation of molecular properties and also don't provide any information about ap-proximations for functionals like $F[n(\vec{r})]$. In the direct comparison to the variational approach of the Hartree-Fock method, the variational principle introduced in the sec-ond theorem of Hohenberg and Kohn is even more tricky. Whereas in wave-function based approaches like Hartree-Fock or configuration interaction [60](CI) the obtained energy value provides information about the quality of the trial wave function (the lower E, the better the wave function), this is not the case in the variational principle based on the electron density. More than that, it can even happen that some functionals provide energies lower than the actual ground state energy in particular calculations [60]. It's also crucial to note that some functions n(r) would satisfy the conditions [71], making them potential ground state densities, but they do not correlate to a potential v(r). The electron density must therefore be v-representable, which means that it must correlate to a certain potential [71].

3.3.3 Advantages and limitations of Hohenberg-Kohn Theorem

Using the variational principle, the Hohenberg-Kohn theorem provides the relationships between density and potential. And just one density is used to determine the ground state energy. Ground state density is what that density is. If there are multiple densities, the density with the lowest energy is the ground state density. The Hohenberg-Kohn theorem only uses one direction in the majority of modern DFT applications, and that direction is utilized to determine the ground state density for a specific system that is characterized by an external potential. For the opposite direction, the inverse problem, it is initially unclear whether there even is a potential that, whether for the interacting or non-interacting system, the v-representability problem, leads to a certain density through the solution of the Schrödinger equation. There have been documented cases of both v-representable and non-v representable densities. The Hohenberg-Kohn theorems therefore need to be v-representable. From density, we determined all of the electrical characteristics. The non-classical phrase cannot be used to characterize the Hohenberg-Kohn theorems. It is difficult to express the functional word accurately. This theorem is invalid if the density is not v-representable. While the Hohenberg-Kohn theorem indicates that the ground state density can be used to compute system attributes, it does not show how to find the ground state density.

3.4 The Kohn-Sham equations

The fact that the energy functional can be reduced to the ground-state energy of a many-electron system is intriguing.

$$E[n] = \int n(r)v(r)dr + F[n] \tag{3.28}$$

Where

$$F[n] = T[n] + V_{ee}[n] \tag{3.29}$$

The ground-state electron density is the density that minimizes $E[n]$ and hence satisfies the Euler equation

$$\mu = v(r) + \frac{\delta F[n]}{\delta n(r)} \tag{3.30}$$

where μ is the Lagrange multiplier associated with the constraint

$$\int n(r)dr = N \tag{3.31}$$

Among all possible solutions of (3.30), one takes that which minimizes $E[n]$. Thomas-Fermi and related models constitute a direct approach, whereby one contructs explicit approximate forms for$T[n]$ and $V_{ee}[n]$. This produces a nice simplicity the equations involve electron density alone. There are5mm seemingly insurmountable difficulties in going beyond the crude level of approximation. In a trade of simplicity for accuracy, Kohn and Sham (1965) invented an ingenious indirect approach to the kinetic-energy functional $T[n]$, the Kohn-Sham (KS) method. They thereby turned density functional theory into a practical tool for rigorous calculations.

Kohn and Sham proposed introducing orbitals into the problem in such a way that the kinetic energy can be computed simply to good accuracy, leaving a small residual correction that is handled separately. To understand what is involved and what Kohn and Sham did, it is convenient to begin with the exact formula for the ground state kinetic energy,

$$T = \sum_{i}^{N} n_i \left\langle \psi_i \left| -\frac{1}{2}\vec{\nabla}^2 \right| \psi_i \right\rangle \tag{3.32}$$

where the ψ_i and n_i are, respectively, natural spin orbitals and their occupation numbers. The Pauli principle requires that $0 \leq n_i \leq 1$; we are assured from the Hohenberg-Kohn theory that this T is a functional of the total electron density

$$n(r) = \sum_{i}^{N} n_i \sum_{s} |\psi_i(r,s)|^2 \tag{3.33}$$

For any interacting system of interest, there are an infinite number of terms in (3.32) or (3.33), which is ponderous at best. Kohn and Sham (1965) showed that one can

build a theory using simpler formulas, namely

$$T_s[n] = \sum_i^N \left\langle \psi_i \left| -\frac{1}{2}\vec{\nabla}^2 \right| \psi_i \right\rangle \tag{3.34}$$

and

$$n(r) = \sum_i^N \sum_s |\psi_i(r,s)|^2 \tag{3.35}$$

Equations (3.34) and (3.35) are the special case of (3.32) and (3.33) having $n_i = 1$ for N orbitals and $n_i = 0$ for the rest; this representation of kinetic energy and density holds true for the determinantal wave function that exactly describes N noninteracting electrons.

We know that any nonnegative, continuous, and normalized density n is N-representable and always can be decomposed according to (3.35). But given a n(r), how can we have a unique decomposition in terms of orbitals so as to give a unique value to $T_s[n]$ through (3.34)? In analogy with the Hohenberg-Kohn definition of the universal functional $F_{HK}[n]$, Kohn and Sham invoked a corresponding noninteracting reference system, with the Hamiltonian

$$\hat{H} = \sum_i^N \left(-\frac{1}{2}{\nabla_i}^2 \right) + \sum_i^N v_s(r) \tag{3.36}$$

in which there are no electron-electron repulsion terms, and for which the ground state electron density is exactly n. For this system there will be an exact determinantal ground state wave function

$$\psi_s = \frac{1}{\sqrt{N!}} det[\psi_1 \psi_2 \dots \psi_N] \tag{3.37}$$

where the ψ_i are the N lowest eigenstates of the one-electron Hamiltonian $\hat{h_s}$:

$$\hat{h_s}\psi_i = \left[-\frac{1}{2}{\nabla_i}^2 + v_s(r) \right] \psi_i = \epsilon_i \psi_i \tag{3.38}$$

The kinetic energy is $T_s[n]$, given by (3.34),

$$T_s[n] = \left\langle \psi_s \left| \sum_i^N \left(-\frac{1}{2}\vec{\nabla}^2 \right) \right| \psi_s \right\rangle$$

$$T_s[n] = \sum_i^N \left\langle \psi_i \left| -\frac{1}{2}\vec{\nabla}^2 \right| \psi_i \right\rangle \tag{3.39}$$

and the density is decomposed as in (3.35). The foregoing definition of $T_s[n]$ leaves an undesirable restriction on the density-it needs to be noninteracting v-representable; that is, there must exist a noninteracting ground state with the given $n(r)$. This restriction on the domain of definition of $T_s[n]$ can be lifted, and $T_s[n]$ of the formequation (3.34) can be defined for any density derived from an antisymmetric wave function. Despite being uniquely defined for any density, the quantity $T_s[n]$ is still not the exact kinetic-energy functional $T[n]$. The brilliant concept of Kohn and Sham (1965) is to construct an interesting problem such that $T_s[n]$ precisely represents its kinetic-energy component. We will observe right away that the resulting theory takes the shape of an independent particle. However, it is accurate.

To produce the desired separation out of $T_s[n]$ as the kinetic energy component,rewrite (3.29) as

$$F[n] = T_s[n] + J[n] + E_{xc}[n] \tag{3.40}$$

Where

$$E_{xc}[n] = T[n] - T_s[n] + V_{ee}[n] - J[n] \tag{3.41}$$

The defined quantity $E_{xc}[n]$ is called the exchange-correlation energy; it contains the difference between T and T_s , presumably fairly small, and the nonclassical part of $V_{ee}[n]$. The Euler equation (3.30) now becomes

$$\mu = v_{eff}(r) + \frac{\delta T_s[n]}{\delta n(r)} \tag{3.42}$$

Where the KS effetive potential is defined by

$$v_{eff}(r) = v + \frac{\delta J[n]}{\delta n(r)} + \frac{\delta E_{xc}[n]}{\delta n(r)} = v(r) + \int \frac{n(r')}{|r - r'|} dr' + v_{xc}(r) \tag{3.43}$$

with the exchange-correlation potential

$$v_{xc}(r) = \frac{\delta E_{xc}[n]}{\delta n(r)} \tag{3.44}$$

We initially do not try to solve equation (3.42) directly because of equation (3.42) is merely a rearrangement of (3.30) and the explicit form of $T_s[n]$ in terms of density is as yet unknown. Rather, we follow the indirect approach designed by Kohn and Sham; The Kohn-Sham treatment runs as follows. Equation (3.42) with the constraint (3.31) is precisely the same equation as one obtains from conventional density functional theory when one applies it to a system of noninteracting electrons moving in the external potential $v_s(r) = v_{eil}(r)$. Therefore, for a given $v_{eff}(r)$, one obtains the $\rho(r)$ that satisfies (3.42) simply by solving the N one-electron equations.

$$\left[-\frac{1}{2}\nabla^2 + v_{eff}(r)\right]\psi_i = \epsilon_i\psi_i \tag{3.45}$$

and

$$n(r) = \sum_i^N \sum_s |\psi_i(r,s)|^2 \tag{3.46}$$

Here, v_{eff} depends on $n(r)$ through (3.44); hence, (3.43), (3.45) and (3.46) must be solved self-consistently. One begins with a guessed $n(r)$, constructs v eff (r) from (3.43), and then finds a new n(r) from (3.45) and (3.46). The total energy can be computed directly from (3.28) with (3.29). Equations (3.44)-(3.46) are the celebrated Kohn-Sham equations. They deserve our careful derivation and analysis, to which we proceed.

3.5 Solving the Kohn-Sham equations

We can solve the Kohn-Sham equations once we have roughly calculated the exchange-correlation energy. The Kohn-Sham equations require self-consistent solutions and have an iterative solution. The Hartree potential and the exchange-correlation potential must be defined, and in order to define the Hartree potential and the exchange-correlation potential, we must be aware of the electron density n(r). The

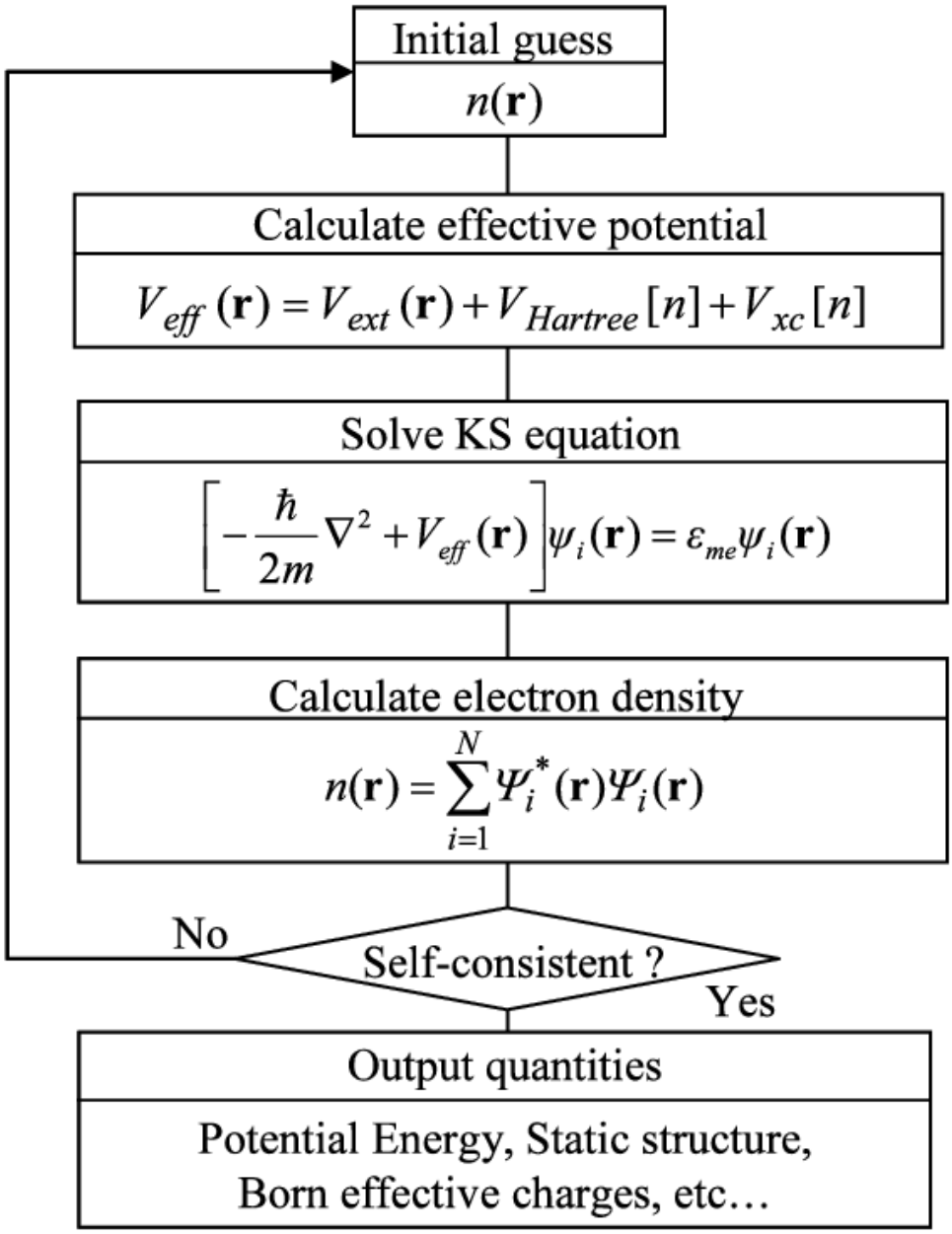

Figure 3.1: Flow-chart-of-solving-the-Kohn-Sham-equation

KS equations offer a mechanism to precisely determine the density and energy of a condensed matter system's ground state using independent-particle techniques. The KS Equations must be consistently solved given the effective KS potential V_{KS} and the constant KS. The terms n(r) and electron density go hand in hand. As seen in Figure 3.1, this is often accomplished numerically by a few self-consistent iterations. Starting with an initial electron density typically a superposition of atomic electron densities the process then calculates the effective KS potential V KS and solves the KS equation using single-particle eigenvalues and wave functions to produce a

new electron density. Self-consistent conditions are then checked. The change in total energy or electron density from the previous iteration, the total force acting on atoms being less than a selected tiny quantity, or a combination of these distinct conditions can be considered self-consistent conditions.f the self consistency is not achieved, the calculated electron density will be mixed with electron density from previous iterations to get a new electron density. A new iteration will start with the new electron density. This process continues until self-consistency is reached. After the self-consistency is reached, various quantities can be calculated including total energy, forces, stress, eigenvalues, electron density of states,band structure, etc. Solving the Kohn-Sham equation with a given Kohn-Sham potential $V_{KS}$is the phase that takes up the most time in the entire procedure. When boundary conditions are used, there are numerous different methods for calculating the independent particle electronic states in solids.

3.6 The Exchange-Correlation Functional in the Kohn Schemes

The ex-change-correlation energy that emerges in the Kohn-Sham formalism and its namesakes, the exchange and correlation energies, have fundamental distinctions that we should also make clear at this point. In Hohenberg Kohn theorem the functional is

$$E[n] = \int n(r)v(r)dr + F[n] \tag{3.47}$$

Where

$$F[n] = T[n] + V_{ee}[n] \tag{3.48}$$

Therefore, Hohenberg Kohn changed the electron's external potential as a result of the nucleus, but this had a constraint regarding how the density would be broken down into a wave function. The absence of a detailed description of electron and electron interaction is another drawback. There are two types of terms in the interaction between electrons: a classical term, or Hartree term, and a non-classical term. The non-classical term that results from resolving several body systems is

valued. There is a correlation among electrons in numerous bodily systems. and produces corelation energy as a result. However, the Hohenberg-Kohn Theorem makes no mention of this. We can now see that for each individual electron orbital that contains an electron, the estimated kinetic energy was defined in terms of the wave function in the Kohn-Sham equations. At the end, they added up all of the electron orbitals for each person, totaling N electron orbitals, each of which takes up $n_i = 1$. In order to calculate the interaction in interacting system, the Hamilton has been built for approximating kinetic energy and effective potential energy of each individual electron from non-interacting system. By adding each hamiltonian created from a single electron, the hamiltonian has finally been created. By resolving the Schrödinger equation, we are able to create the ground state wave function and ground state energy for a variety of bodily systems. However, there is no precise explanation of how electrons and electrons interact in external potential.

The universal functional equation (3.40) in the Kohn-Sham scheme has a non-classical term that refers to the exchange correlation of fermions (electrons) in many-body systems. In the Khon-Sham Theorem, the precise kinetic energy of electrons and the total amount of electron-electron interaction (V ee potential term) cannot be calculated. Therefore, the definition of $E_{xc}[n]$ in equation (3.41) includes the difference between the exact kinetic energy of electrons and the approximate kinetic energy (in a reference frame without interaction) as well as the difference between the electron-electron interaction term and the traditional Hartree term. Since only we are capable of calculating $T_n]$ roughly, the exchange correlation energy has up until now been hampered by problems with the classical coulomb interaction. Because the true shape of the exchange-correlation functional is unknown, it's difficult to solve the Kohn-Sham equations. Two basic approximation methods have been implemented to approximate the exchange-correlation functional. The local density approximation (LDA) is he first effort to estimate the exchange-correlation functional in DFT computations. The second well-known class of approximations to the Kohn-Sham exchange-correlation functional is the generalized gradient approximation (GGA). In the GGA approximation, the local electron density and local gradient in the electron density are included in the exchange and correlation energies [92].

3.6.1 Local Density Approximation (LDA)

The exchange-correlation functional (LDA) is most easily approximated by the local density approximation. According to the local density approximation, the energy density of a homogeneous electron gas with the same electron density n(r) at every site in the molecule has the value that would be provided by a homogeneous electron gas with the same electron density n(r) at that place. Using the presumption that a derivative is a nonlocal characteristic, the word "local" was created to distinguish the technique from those in which the functional is dependent both on r and on the gradient (first derivative) of r. The local approximation is only practical in theory for slowly varying densities. Despite the fact that atom and molecule densities are sometimes exceedingly uneven, LDA nevertheless produces excellent results. Findings from LDA for equilibrium structures, harmonic frequencies, and dipole moments in molecules have been shown to be generally satisfactory [93]. The KS equations (3.43), (3.45) and (3.46) while exactly incorporating the kinetic energy $T_s[n]$, still leave the exchange-correlation functional E xc [n] of (3.40) unsettled.An explicit form for E xc [n] is needed to specify the KS equations. The search for an accurate $Exc[n]$ has encountered tremendous difficulty and continues to be the greatest challenge in the density-functional theory. We describe in this section the simplest approximation, the local approximation proposed by Kohn and Sham (1965). The Thomas-Fermi functional for kinetic energy and the Dirac functional for exchange energy were locally obtained using the uniform-electron-gas formula. We can apply the uniform-electron-gas formula only for the unknown portion of the remaining energy functional now that the kinetic energy $T_s[n]$ has been thoroughly dealt in the KS scheme. The local-density approximation (LDA) for exchange and correlation energy is thus introduced.

$$E_{xc}^{LDA}[n] = \int n(r)\epsilon_{xc}(n)dr \tag{3.49}$$

where $\epsilon_{xc}(n)$ indicates the exchange and correlation energy per particle of a uniform electron gas of density n. The corresponding exchange correlation potential of (3.43)

then becomes

$$v_{xc}^{LDA}(r) = \frac{\delta E_{xc}^{LDA}}{\delta n(r)} = \epsilon_{xc}(n) + n(r)\frac{\delta \epsilon_{xc}(n)}{\delta n} \tag{3.50}$$

and the KS orbital equations read

$$\left[-\frac{1}{2}\nabla^2 + v(r) + \int \frac{n(r')}{|r-r'|}dr' + v_{xc}^{LDA}(r)\right] \tag{3.51}$$

The Kohn-Sham local density approximation (KS-LDA), often known as the LDA approach in the literature, is defined by the self-consistent solution of (3.51).

3.6.2 Generalized-Gradient Approximation (GGA)

In many circumstances, the creation of multiple generalized-gradient approximations (GGAs)that include density gradient corrections and larger spatial derivatives of the electron density outperforms LDA. Becke (B88), Perdew, et al, and Perdew, Burke, and Enzerhof are three of the most extensively utilized GGAs (PBE). The definition of the XC energy functional of GGA is the generalized form of LSDA to include corrections from density gradient $n(r)$as

$$E_{xc}^{GGA}[n_\uparrow(r), n_\downarrow(r)] = \int n(r)\epsilon_{xc}^{hom}(n_\uparrow(r), n_\downarrow(r), |\nabla n_\uparrow(r)|, \nabla n_\downarrow(r)|, \ldots\ldots)dr$$

$$= \int n(r)\epsilon_{xc}^{hom}(n_\uparrow(r), n_\downarrow(r), |\nabla n_\uparrow(r)|, \nabla n_\downarrow(r)|, \ldots\ldots)dr \tag{3.52}$$

Where F_{XC} is dimensionless and $\epsilon_X^{hom}(n(r))$ is the exchange energy density of the unpolarized HEG. F_{XC} Can be decomposed linearly into exchange contribution F_X and correlation contribution F_C as $F_{XC} = F_X + F_C$. For a detailed treatment of F_X and F_C indifferent GGAs. GGA beats LDA in forecasting molecular bond length and binding energy, crystal lattice constants, and other parameters in general, especially in systems with rapidly changing charge density. When the lattice constants from LDA calculations match actual data well, but GGA overestimates it, GGA overcorrects LDA results in ionic crystals

Chapter 4

Computational details

In the present work, first principle calculations of K_2TeCl_6 are done using DFT based computational WIEN2k code. For this purpose, full potential linearized augmented plane-wave (FP-LAPW) method is used to study their structural, electronic, elastic, and optical properties [94]. Also investigate the vacancy ordered double perovskite K_2TeCl_6 under different pressure with respect to its electronic, optical and mechnical properties. Firstly,using Perdew-Burke-Ernzerhof,and Generalished Gradient Approximation (PBE-GGA),electronic structures are optimized for reducing the inter-atomic forces to stablize the structure [95]. We have optimized the structure of K_2TeCl_6 through energy minimization where we calculate the lattice parameters umder pressure like 0, 30, 60, 90, 120, 150, 180, 210 for each component respectively. The energy convergence criterion was set to 10^{-5} Ry. The unit cell is separated into the interstitial region and non-overlapping atomic spheres centered at the atomic sites in the FP-LAPW approach. The exchange and correlation potential energies in the Kohn-Sham equation had been approximated using the Perdew-Burke Ernzerhof generalized gradient approximation (GGA).

In FP-LAPW method, the basis set size in the interestial region is represented by as $R_{MT} \times K_{MAX}$, Where R_{MT} and K_{MAX} are smallest muffin-tin-radii and maximum plane-wave cut-off,respectively. We set $R_{MT} \times K_{MAX} = 8$ for all calculation and

the convergence of the basis set was controlled by the cut-off parameter -6 Ry. The charge density and the potential in the interstitial region had been expanded as a Fourier series with the largest wave vectors up to $G_{max} = 16$. The charge convergence is selected as 0.0001 e and energy convergence 0.00001 Ry during self-consistency cycles. DFT calculations being sensitive to the choice of K-points,are performed using for SCF, Band structure, and mechanical calculations, there are 4000 k-points in the brillouin zone, while there are 20000 for calculations of DOS and optical characteristics. From the strain as a function of volume, the elastic constants C_{11}, C_{12} and C_{44} were determined under ambient and uniform different pressure. According to characteristics of the cubic lattice's symmetry, the elastic constants can be determined via the IRelast program as C_{11}, C_{12}, and C_{44}, which are three independent constants. The structure and outputeos files have been kept in a directory and applied the command for calculating elastic constant. Conventionally the stability conditions of the elastic constants for cubic crystal are $C_{11} - C_{12} > 0$, $C_{11} > 0$, $C_{44} > 0$, $C_{11} + 2C_{12} > 0$, $C_{12} > B > C_{11}$.C_{11} represent resistance in x-direction under linear compression [96]. Similarly, C_{44} indicates the resistance to shear deformation under applied shear stress. In general, we state that C_{44} is concerned with the hardness of the materia [97]. For both examined compounds, the value of C_{12} is negative, which shows the reduction in transverse expansion when stress is applied. From elastic constants (C_{11}, C_{12}, C_{44}), we can easily determine the elastic moduli, such as Young's modulus (Y), bulk modulus (B), and shear modulus (G), by using Voigt-Reuss-Hill approximation [98] [99]. From elastic constants (C_{11}, C_{12}, C_{44}) we can easily determine the elastic moduli, such as Young's modulus (Y), bulk modulus (B), and shear modulus (G), by using Voigt-Reuss-Hill approximation.

$$B = \frac{1}{3}(C_{11} + 2C_{12}) \tag{4.1}$$

$$Y = \frac{9BG_V}{3B + G_V} \tag{4.2}$$

$$G = \frac{1}{2}(G_V + G_R) \tag{4.3}$$

Where, G_V and G_R are the Voigt shear modulus and Reuss shear modulus, respec-

tively, and are determined by using the following relation [99]

$$G_V = \frac{1}{5}(C_{11} - C_{12} + 3C_{44}) \tag{4.4}$$

$$G_R = \frac{5C_{44}(C_{11} - C_{12})}{3(C_{11} - C_{12}) + 4C_{44}} \tag{4.5}$$

The elastic anisotropy factor, 'A' that gives vital particularities on structural stability is obtained from

$$A = \frac{2C_{44}}{C_{11} - C_{12}} \tag{4.6}$$

Regarding full isotropic materials, 'A' is equal to one. That makes deviation from the anisotropy of crystal.and anisotrophy constant can be defined by

$$A_G = \frac{(G_V - G_R)}{(G_V + G_R)} \tag{4.7}$$

When $G_V = G_R$, the $A_G = 0$, which impiles the full isotropy, since A_G obtains from zero, we get higher anisotropy. Bulk modulus is used to calculate the resistance to volume changes under pressure [100]and maybe simply computed using elastic constants from Equation (4.1). Furthermore, Young's modulus (Y) is used to predict a material's stiffness whereas shear modulus (G) is a proportion of resistance to reversible deformation under shear stress that helps to define a material'sm hardness more precisely than the bulk modulus. Pugh's ratio (B/G) is used to determine a material's brittleness or ductility [99]. If the B/G ratio is more than 1.75, the compound is ductile; otherwise, it is brittle. The Poisson's ratio $v > 0.26$ for materials act like as ductile fashion and otherwise brittle fashion. For perfectly elastic isotropic regions and perfectly incompressible material takes the ν values 0.25, 0.5 correspondingly.

Chapter 5

Results and Discussion

5.1 Structural Properties

The crystallographic structures along with the first Brillion zone for vacaency ordered cubic 225 ($Fm\bar{3}m$) double perovskite K_2TeCl_6 are presented in Figure 5.1. The geometrical structure contains octaheddron of $TeCl_6$ with interstitial sites filled by K atoms. The octahedrons are seperated by 12-fold coordinates of Cl atoms. Figure 5.1 shows that K and Te atoms are surronded by 12 and 6 halogen respectively. In this cubic structural arrangements of atoms K, Te, and Cl atoms occupy 8c, 4a, and 24e Wyckoof sites with fractional coordinates (1/4, 1/4, 1/4), (0, 0, 0) and (0.24, 0, 0), respectively [101]. The optimization plots for total energy versus volume after fitting with Murnaghans equation of states. It is evident that the minimization of energy is held at the lowest point of Figure 5.2. For meaningful discussion of the physical properties, evaluation of stability conditions for the structure and dynamic nature is important. The structrual stability of vacancy ordered double perovskites has been confrimed by computing Goldschmidt tolerance factor that is mathmatically expressed as

$$t_f = \frac{(r_K + r_{Cl})}{\sqrt{2}(r_{Te} + r_{Cl})}. \tag{5.1}$$

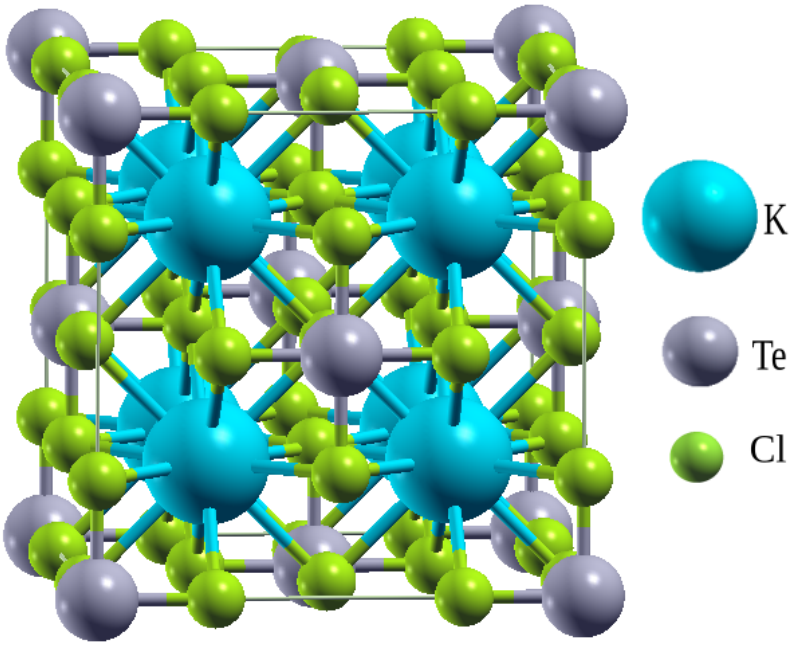

Figure 5.1: Crystal structure of cubic K_2TeCl_6 vacancy ordered double perovskite.

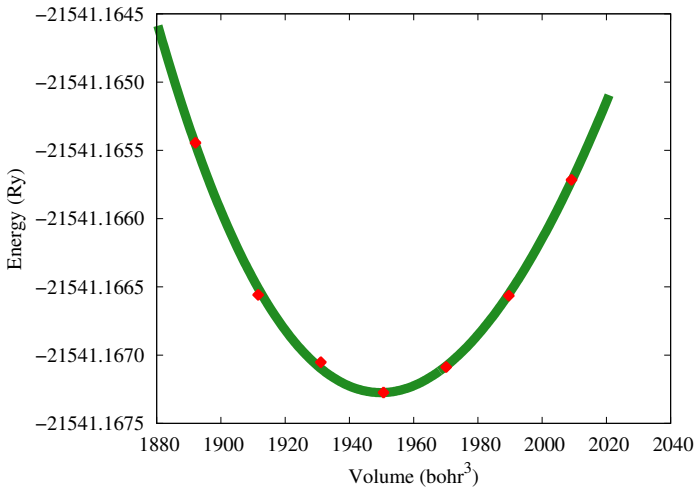

Figure 5.2: The optimized energy verse volume optimization plots of K_2TeCl_6.

where r_{Cl}, r_{Te}, and r_K are radii of Cl, Te, and K atoms, respectively. The ideal value of tolerance factor for cubic perovskite is 1.0. However, the range of T_f from 0.96 to 1.04 is also considered best. The reported values of K_2TeCl_6 is 0.98. The value of tolerence factor expressing structrual stability of the cubic materials is unity, and deviated values indicate structrual instability [102].

5.2 Elastic property

The elastic properties of materials provide a necessary knowledge on their mechanical strength also the elastic constant gives us a better ability to understand how the solid mechanical stability can change under the forces. We investigate elastic constants (C_{11}, C_{12}, C_{44},) under ambient conditions for K_2TeCl_6. The existence of the crystal isn't possible in the stable or meta-stable state unless its elastic constants obey the generalized mechanical stability criteria [103]. Our calculated values of the elastic constants and Bulk moduli properly follow the cubic stability criteria. From the values of the elastic constants, mechanical properties like Young's modulus (Y), which presents the strength of the material; the bulk modulus (B), which describes the stiffness of a material, higher the value of B, the higher its stiffness resistance is; and the shear modulus (G),which describes the calculated plastic twist of a material. The obtained value of the shear modulus is 13.457 GPa, which is small, meaning that the compound shows less plastic twist. The value of Young's modulus (Y) was obtained from the bulk modulus (B) and the shear modulus (G). In order to define the ductile or brittle behavior of K_2TeCl_6,we obtained the B/G ratio, which was calculated to be 2.098 and shows a ductile nature. An estimation of ductility and brittlenesscan also be obtained from the Cauchy pressure value (C_{12}–C_{44}); positive values characterize a material as ductile and negative values as brittle. From the information in Table 5.1, it is clear that the Cauchy's pressure is positive for K_2TeCl_6, which emphasize its ductile nature. Poisson's ratio ν is another rule utilized for determining the ductility and brittleness of a compound. If its value is greater than 0.26, the material possesses ductile nature; otherwise, the material is considered to be brittle. Table 5.1 shows that Poisson's ratio for K_2TeCl_6 is close to 0.26, which confirms its ductile nature. Poisson's ratio ν' also gives knowledge about the bonding forces available in solid materials. For central force solids, Poisson's ratio has a range of 0.25 to 0.5. From the data in Table 5.1, it is clear that our computed Poisson's ratio lies in this range, implying that the bonding forces are of central types. As per our insight, no theoretical or experimental data exist in the literature on this compound for elastic properties to which we can compare our work. We believe that our work can stimulate further research in this direction in the future. Furthermore,

Table 5.1: lattice constant (a_0), Band gap, the estimated elastic constant C_{11}, C_{12}, and C_{44}, the bulk modulus(B), the elastic anisotropy factor (A), the percentages of anisotropy (A_G), Cauchy's pressure, Youngs Modulus (Y), the shear modulus(G), B/G ratio and Poissons ratio (ν) for K_2TeCl_6 at ambient pressure.

Specification	K_2TeCl_6
a_0	10.50
Band gap (eV)	2.622
$C_{11}(GPa)$	61.36
$C_{12}(GPa)$	11.67
$C_{44}(GPa)$	8.70
B(GPa)	28.23
A	0.350
A_G	0.126
Cauchy's pressure	2.97
Y(GPa)	38.57
G(GPa)	13.45
B/G	2.09
ν	0.294

The mechanical properties and structural stability of a material are often assessed using the elastic constants. The elastic nature describes how a material deforms under strain before recovering and returning to its original shape once the load is removed. It is important to reveal information about the binding properties between adjoining atomic planes, the anisotropic nature, and structural stability. A cubic compound has three independent elastic constants: C_{11}, C_{12}, and C_{44}. Table 5.2 lists the computed C_{11}, C_{12},C_{44} , and Cauchy pressure ($C_{12} - C_{44}$) for K_2TeCl_6 compound under pressure. The calculated elastic constants suggest that the studied

Table 5.2: Calculated the estimated elastic constant C_{11}, C_{12}, and C_{44}, Cauchy's pressure $(C_{12} - C_{44})$ of K_2TeCl_6 at various applied pressures.

Pressure(GPa)	C_{11}	C_{12}	C_{44}	$C_{12} - C_{44}$
0	61.36	11.67	8.70	2.97
30	152.53	25.36	13.47	11.88
60	188.26	29.92	10.19	19.72
90	212.82	32.74	10.97	21.77
120	231.97	34.86	12.60	22.25
150	247.63	36.66	11.39	25.27
180	261.39	38.22	12.06	26.16
210	273.82	39.47	12.57	26.90

compound is mechanically stable even under applied pressure. In addition, $(C_{12} - C_{44})$ can identify the brittleness and ductility of materials. If $(C_{12} - C_{44})$ possesses a positive (negative) value, the material should be ductile (brittle). Therefore, the titled compound is expected to be ductile because of having positive values of $(C_{12}-C_{44})$ Table 5.2. Increasing pressure, this compound is slightly more effective for ductility. Various fundamental mechanical properties, including the bulk modulus B (GPa), the shear modulus G (GPa), Youngs Modulus Y (GPa), the elastic anisotropy factor (A), the percentages of anisotropy (A_G), B/G ratio and Poissons ratio (ν) of K_2TeCl_6 at various applied pressures are determined using the estimated elastic constant and presented in Table 5.3. The B and G stand for fracture resistant and plastic deformation, respectively. Y is a measure of material's stiffness and has proportional relationship. However, the application of pressure induces more resistance to fracture and plastic deformation as well as makes them stiffer than that exhibited by the compounds without pressure. The critical value of ν to distinguish a materials' ductile or brittle nature is 0.26. A material is said to be ductile if ν is larger than 0.26. Thus, K_2TeCl_6 compound is concluded as ductile materials Table

Table 5.3: The calculated the bulk modulus B (GPa), the shear modulus G (GPa), Youngs Modulus Y (GPa), the elastic anisotropy factor (A), the percentages of anisotropy (A_G), B/G ratio and Poissons ratio (ν) of K_2TeCl_6 at various applied pressures

Pressure(GPa)	B	G	Y	A	A_G	B/G	ν
0	28.23	13.45	38.57	0.350	0.126	2.098	0.294
30	67.75	26.59	86.32	0.211	0.260	2.547	0.326
60	82.70	26.71	98.37	0.128	0.414	3.094	0.354
90	92.77	29.76	110.83	0.121	0.431	3.117	0.355
120	100.56	33.17	121.96	0.127	0.416	3.034	0.351
150	106.99	33.37	127.59	0.107	0.469	3.205	0.358
180	112.61	35.31	134.90	0.108	0.468	3.189	0.358
210	117.53	36.96	141.33	0.107	0.471	3.179	0.357

5.3. Another essential feature is B/G, which has a crucial value of 1.75 to divide solid materials into ductile or brittle. The calculated values of B/G also reveal the ductile behavior Table 5.3.

5.3 Electronic property

To observe the potential area for practical applications of the studied compounds investigating the band structure and density of states. The knowledge of electronic band structures and density of states plays a prominant role for understading the physical properties of any material. The calculated band structure plotted along with high symmetry directions in the first Brillion zone and density of states are presented in Figure 5.3 and Figure 5.4 respectively. The ability to classify materials such as metals, semimetals, insulator, and semiconductor requries an understanding of electronic band structure. The valance band maxima lie at W or X symmetry directions, while conduction band minima lie at L symmetry direction in the first Brillion zone. Thus from band structures it is evident that the K_2TeCl_6 perovskite

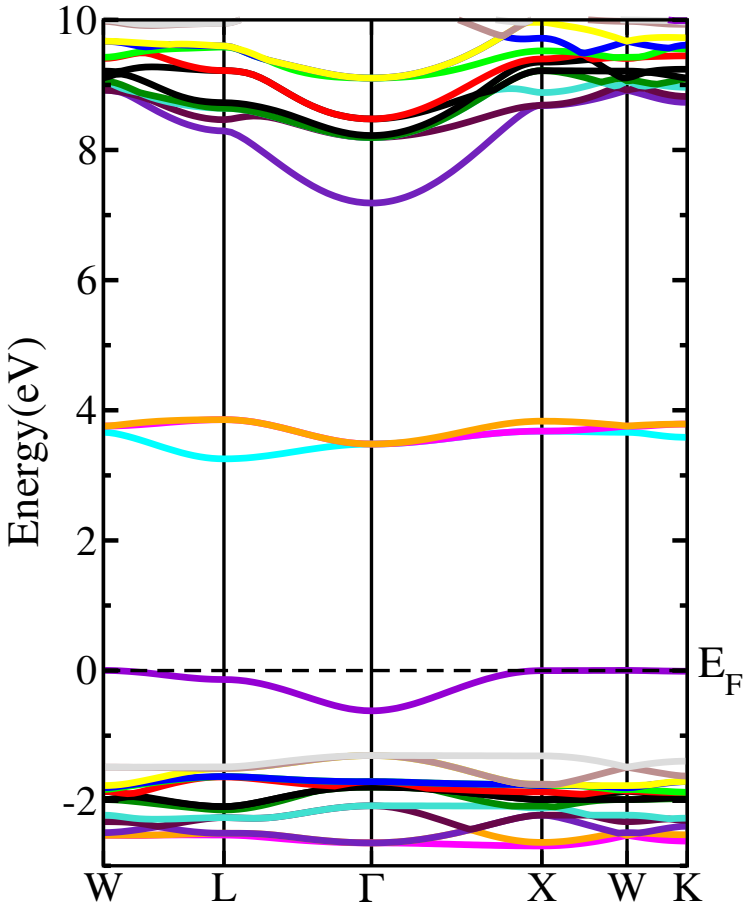

Figure 5.3: Band structure plotted using PBE approximation of K_2TeCl_6 at ambient pressure.

derivatics represent indirect band gap semiconductor because the top of valance bands and the bottom of conductions band are located in different direction in first Brillion zone. The band gap calculated for K_2TeCl_6 is 2.622 eV at ambient pressure. Because holes have a somewhat higher effective mass than electrons, there are more states at the valance band edge (which is significantly closer to the fermi level) than in the conduction band. As a result, the investigated double perovskite seems to exhibit p-type nature. Figure 5.4(a) represent the total density of states for K_2TeCl_6, the contribution of elements mainly lies below the fermi level compared to avobe fermi level. Figure 5.4 (b,c,d) illustrates the partial density of states of K_2TeCl_6 which are plotted, see the role of sublevels in the hybridization. The density of states and Band structure have small difference because of theoritical approximations in DFT calculations. In this energy, hybridization among p-states of Cl, p-state of Te and traces of s-states of K occurs. From Figure 5.4(a), Dos

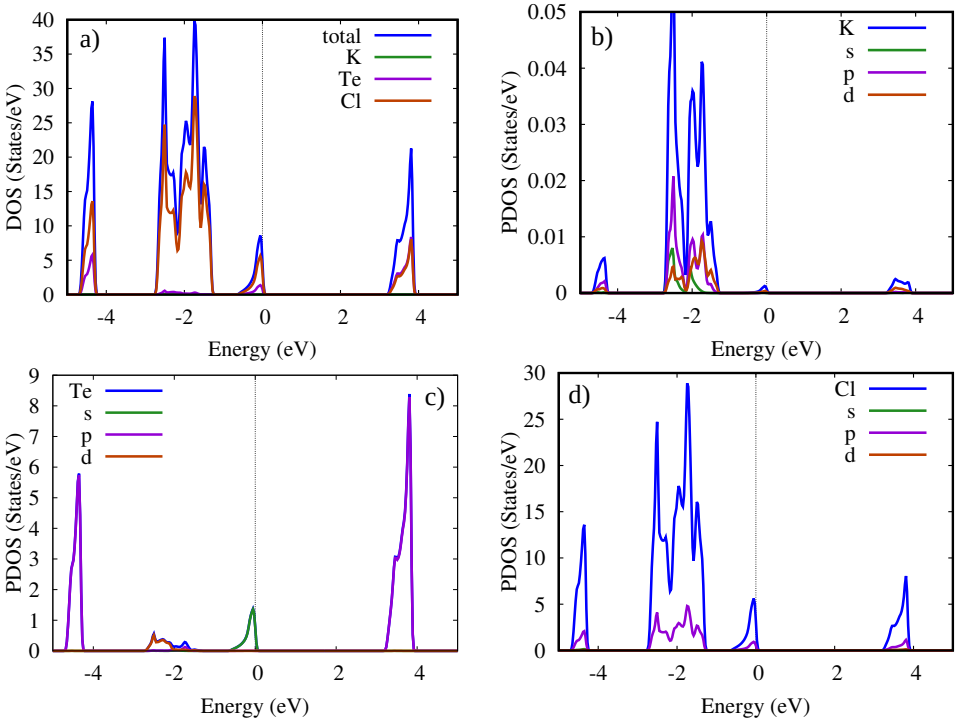

Figure 5.4: a) Total density of states of K_2TeCl_6, b) Partial density of states of K, c) Partial density of states of Te, d) Partial density of states of Cl at ambient pressure.

Table 5.4: Change of lattice parameter and band-gap under different pressure

Pressure(GPa)	Lattice parameter(a_0)	Band-Gap(eV)
0	10.50	2.622
30	9.65	2.438
60	9.44	2.267
90	9.31	2.137
120	9.22	2.032
150	9.15	1.943
180	9.10	1.865
210	9.06	1.797

contribution in the valance band region is higher than the conduction band. We get the higher peak of density of states in the valance band. In K_2TeCl_6 systems the Cl atom contribution in the density of states is higher than other atoms. The energy region -4.5 eV to -5.0 eV reveals hybridization between Cl-3p and Te-4p states. On the other hand,in conduction band contains the energy ranges 3.0 eV to 4 eV hybridization occurs between Cl-3p and Te-4p states. The effect of different pressure on the electronic properties have also been studied comprehensively by the PBE-approximation method. It is very important to check the effect of pressure on

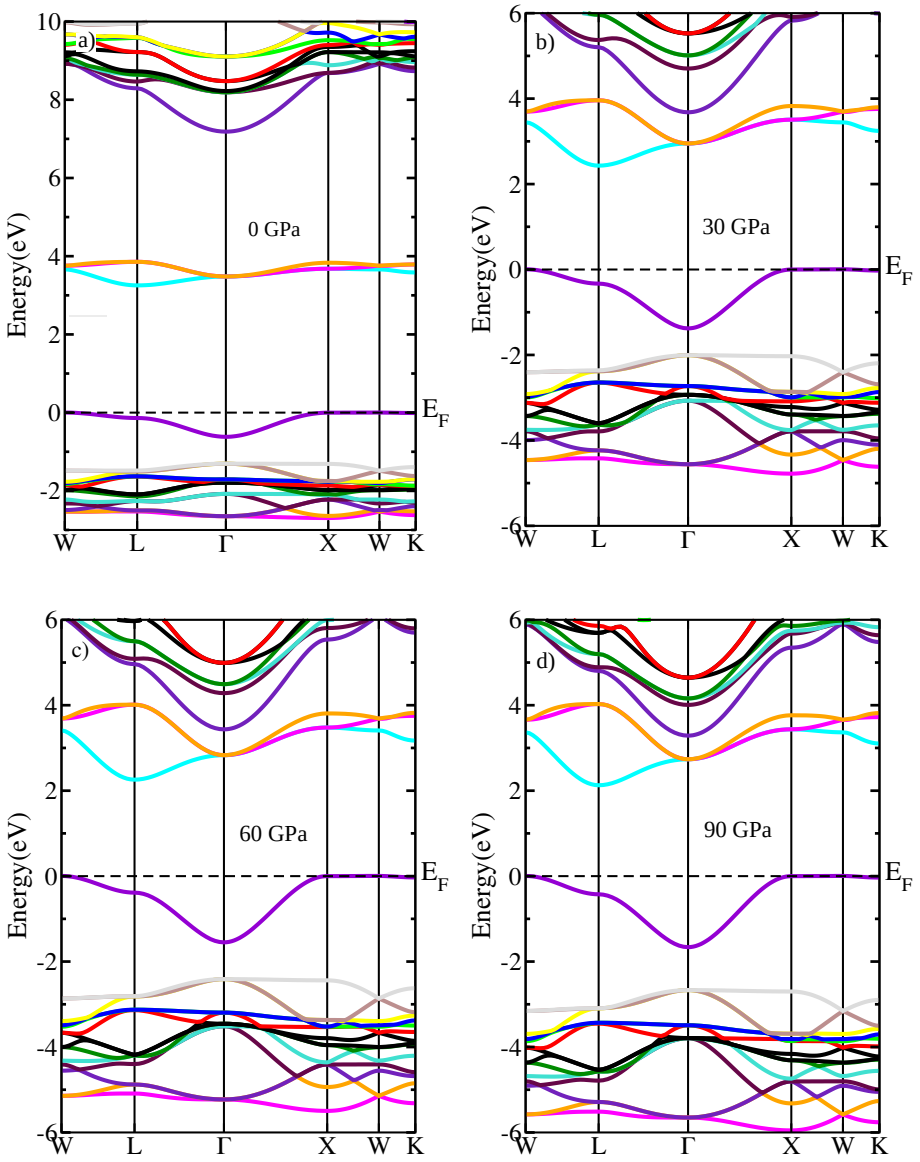

Figure 5.5: Band structure of K_2TeCl_6 vacancy ordered double perovskite under (a) 0 GPa (b) 30 GPa (c) 60 GPa (d) 90 GPa pressure.

electronic properties,which in turn gives us information about surface properties. Effect of pressure on electronic properties has been studied intensively by reducing the lattice parameter from its equilibrium value. We conducted band-gap calculations under varying pressures to investigate the response of our compound to pressure changes. The variation of band gap under different pressure has shown in Table 2.1. The lattice constant decreases as the pressure increases, as seen by the data in the table. The calculated band structures,along with high symmetry directions of BZ are reported in Figures 5.5 and 5.6 under different pressures. The horizontal line

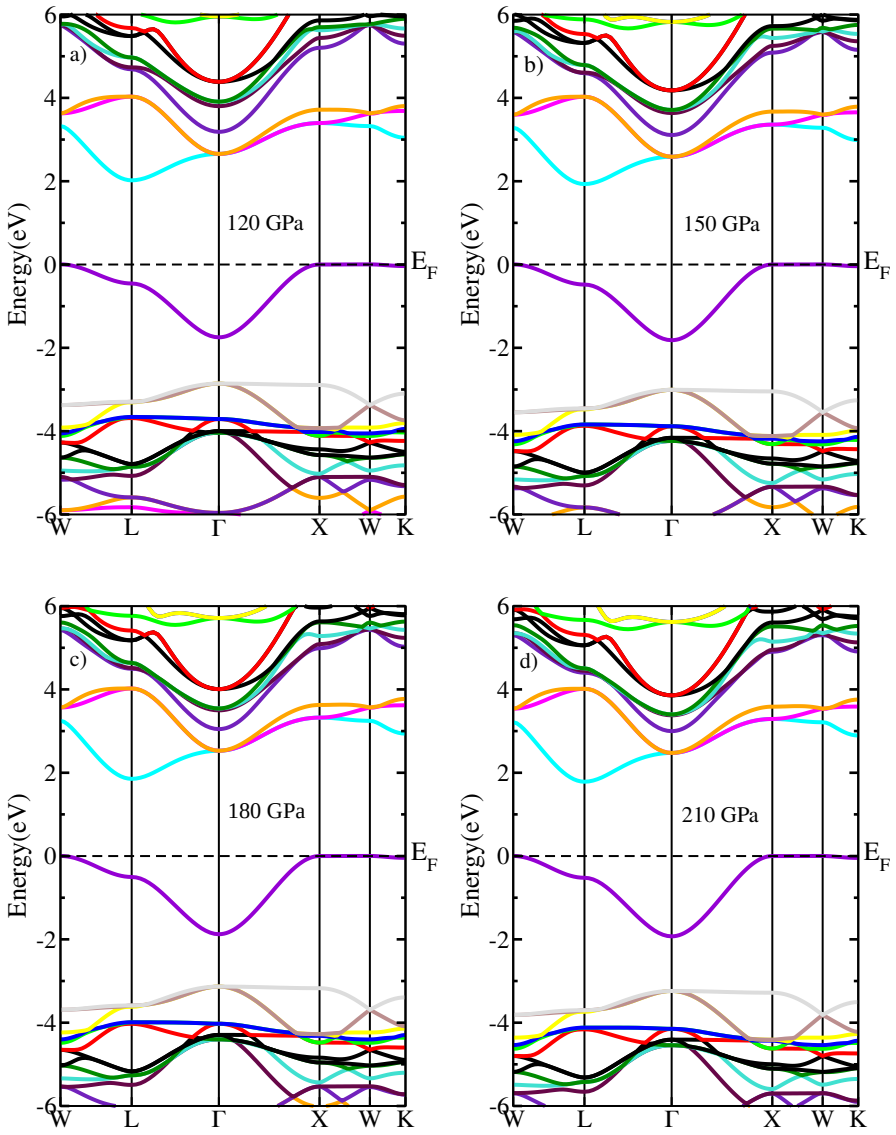

Figure 5.6: Band structure of K_2TeCl_6 vacancy ordered double perovskite under (e) 120 GPa (f) 150 GPa (g) 180 GPa (h) 210 GPa pressure.

at 0 eV denotes the fermi level for all pressure. For K_2TeCl_6 compounds at 0 GPa there is a indirect band gap of 2.622 eV as valence band maxima and conduction band minima are located in different direction in first Brillion zone. On applying the pressure, the band gap significantly reduces because of the expansion in the energy bands. At 30 GPa, band gap increase an amount of 2.438 eV compared to 0 GPa. As the pressure is increased up to 210 GPa, the band gap significantly reduces to value of 1.797 for K_2TeCl_6. Accordingly, it can be said that when pressure increases, a growing number of electrons shift from the valence to the conduction bands, enhancing conductivity and other optoelectronic properties that are better

suited for device application. To strongly understand the electronic properties of the material of interest, We have computed the total density of states and partial density of states using PBE. At different pressures, we draw diagrams representing the density of states. It has been observed that the density of states at the fermi level changes as the pressure changes.We may compare it to band-gap since pressure changes cause a change in the band-gap. So the energy distance between the conduction band and valance band from Fermi lebel is also change. The total density of states of pressurized K_2TeCl_6 is computed and depicted in Figure 5.7(a) as compared ambient pressure in order to clarify the potential electrical transition from the valence to the conduction band and recombination among the component states. The vertical dashed line at 0 eV denotes the fermi energy E_F. The total density of

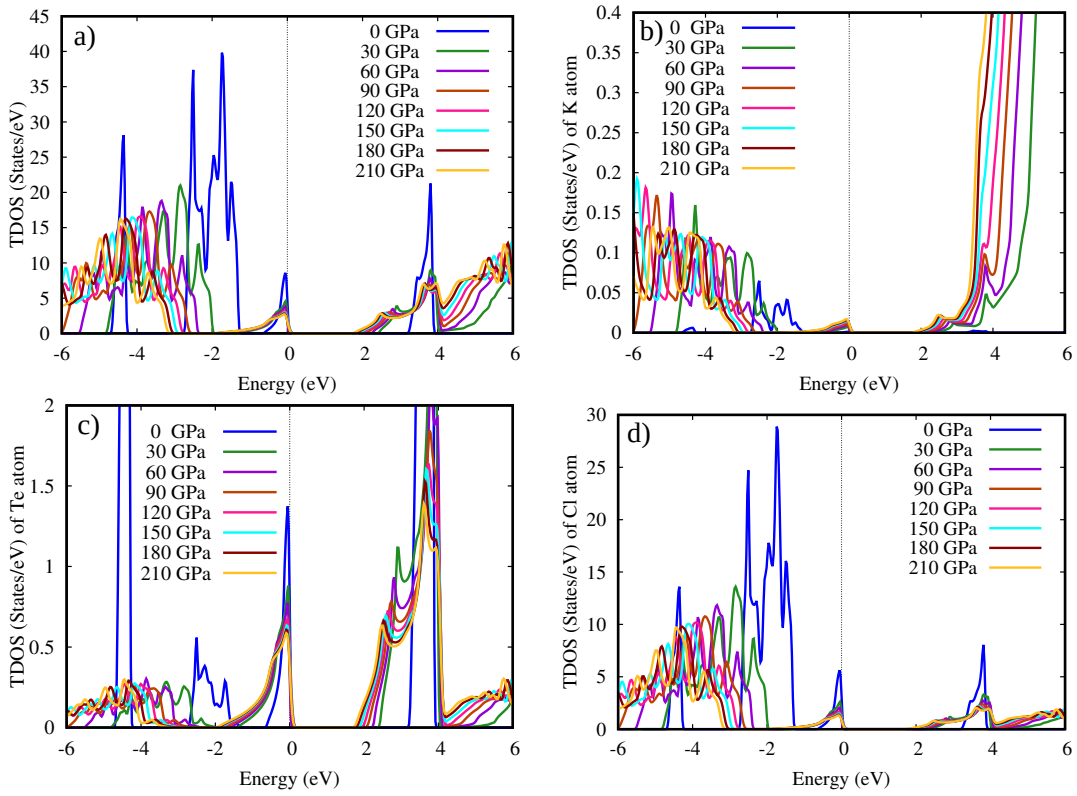

Figure 5.7: a)Total density of states of K_2TeCl_6 vacancy ordered double perovskite, b)Total density of states of K atom, c) Total density of states of Te atom, d)Total density of states of Cl atom at ambient and different pressure.

states of pressurized K_2TeCl_6 is computed in Figure 5.7(a) as compared to 0 GPa and shows that all sharp peak subjected to pressure gradually move downward and the topmost valence electronic states in the regiopn of -2 to -4 eV shift to 2 to 6 eV

in the conduction band. Figures 5.7(b,c,d) illustrate the total density of states representing the contribution of individual atoms in both ambient and uniform pressure conditions.

5.4 Optical property

The optical characteristics of the considered K_2TeCl_6 include dielectric function, absorption coefficient, optical condutivity, reflectivity,and refractive index. The optical characteristics of a materials are very important for its probable use in IR, electronic,and optical applications. The type of interaction between the incident electrmagnetic frequency and the bound lattice constant (a_0) electrons in the valence band affects the optical response. The type of the recombination is used to assess the potential of the materials for optoelectronic applications as the bound electrons absorb the incident energy and transition to the conduction band [104, 105]. All optical parameters were calculated for K_2TeCl_6 double perovslites are plotted against to 0-12 eV energy. The real dielectric function $\varepsilon_1(\omega)$ as well as imaginary dielectric function $\varepsilon_2(\omega)$ of K_2TeCl_6 is presented in Figure 5.8 and 5.9 respectively.

5.4.1 Dielectric Function

The dielectric function $\varepsilon(\omega)$ is very useful for describing the optical nature of given material and different optical variables. The dielectric function is represented by

$$\varepsilon(\omega) = \varepsilon_1(\omega) + i\varepsilon_2(\omega). \tag{5.2}$$

where $\varepsilon_1(\omega)$ and $\varepsilon_2(\omega)$ are the real and imaginary components of the dielectric function,respectively. The real part of the dielectric constant illustrates the light polarization, while the imaginary part show light absorption by the materials. The static values of $\varepsilon_1(\omega)$ are releated with the threshold values for optical absorption (optical bandgap E_g according to penn's model that is reoresented as $\varepsilon_1(0) \approx 1 + (\hbar\omega_p/E_g)^2$, here ω_p and $\hbar$ are plasma resonance frequency and plancks constant, respectively [106]. The $\varepsilon_1(\omega)$ and $\varepsilon_2(\omega)$ are related through Kramer-Kroning relation

[107].

$$\varepsilon_1(\omega) = 1 + \frac{2}{\pi} P \int_0^{\infty} \frac{\omega' \varepsilon_1(\omega')}{\omega' 2 - \omega^2} d\omega'. \tag{5.3}$$

$$\varepsilon_2(\omega) = \frac{e^2 h'}{\pi m^2 \omega^2} \sum_v c \int_{BZ}^{\infty} |M_{cv}(k)|^2 \delta[\omega_{cv}(k) - \omega] d^3k. \tag{5.4}$$

where P and k show principle quantum number and wave vector, respectively. The h is planks constant, ω is the angular frequency, and M is molar mass. The Figure

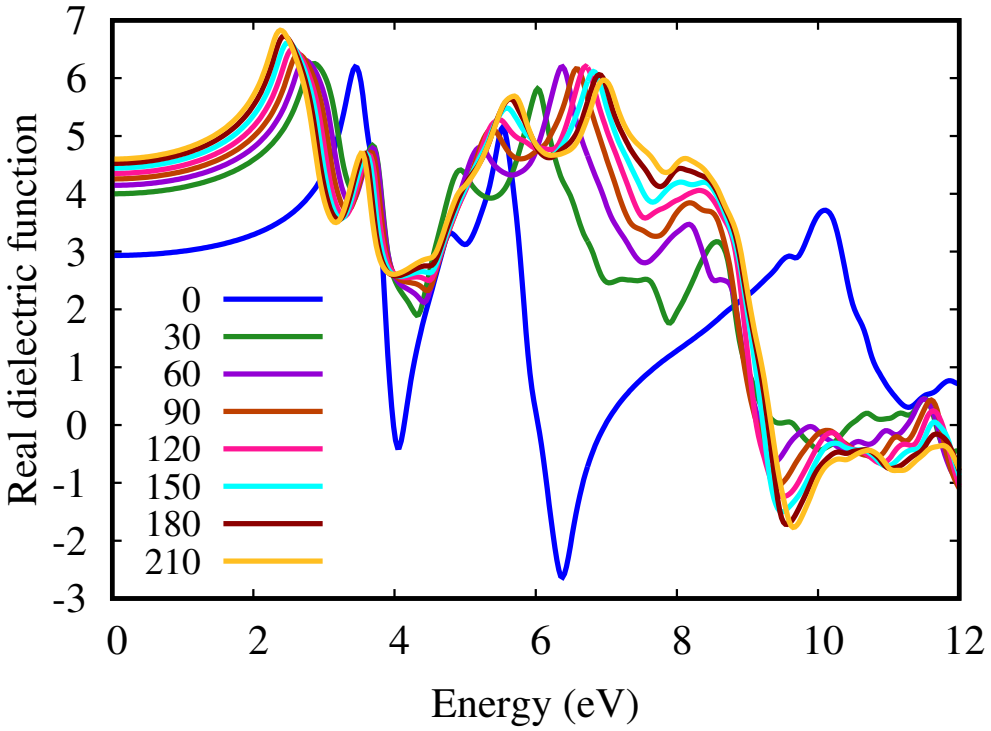

Figure 5.8: Real dielectric function of K_2TeCl_6 vacancy order double perovskite under 0, 30, 60, 90, 120, 150, 180, 210 GPa hydrostatic pressure.

5.8 shows variation of real dielectric constant $\varepsilon_1(\omega)$ with energy. The $\varepsilon_1(\omega)$ exhibites 3 eV for static dielectric constant $\varepsilon_1(0)$ and increases with the energy of the incident electromagnetic wave. From the graph it is evident that $\varepsilon_1(\omega)$ first increases with energy and after getting a peak value it is decreases. The negative $\varepsilon_1(\omega)$ expresses that the typical semiconductor behavior is changed into metallic behavior in the studied vacancy order perovskite. The pressure dependency dielectric constant of K_2TeCl_6 vacancy order perovskite has shown in Figure 5.8 and 5.9 respectively. At 0 GPa, the static part of $\varepsilon_1(\omega)$, expressed as $\varepsilon_1(0)$, is 3 at 0 eV, and it improves with

energy and attains a maximum around 3.24 eV. Interestingely, decreasing band gap due to the applied increasing pressure shifts this maximum to the higher energy, as is evident in Figure 5.8, illustrating the tunable transparency for the visible radiations suggest potential optical applications. The variation of imaginary dielectric function $\varepsilon_2(\omega)$ plotted against the energy range 0-12 eV is shown in Figure 5.9. The

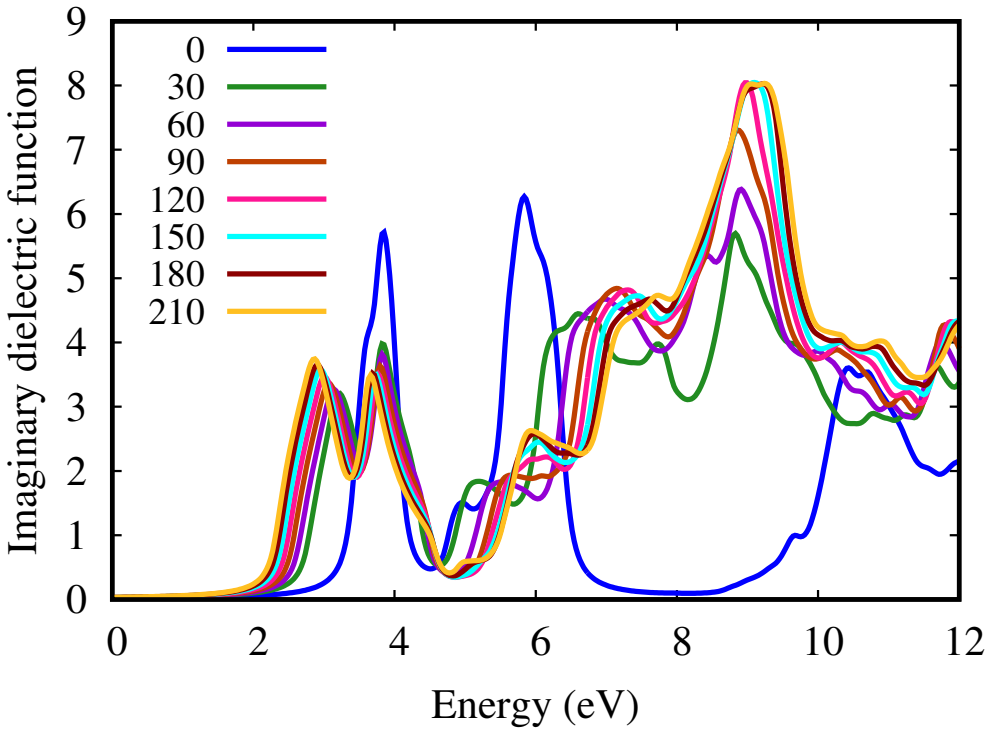

Figure 5.9: Imaginary dielectric function of K_2TeCl_6 vacancy order double perovskite under 0, 30, 60, 90, 120, 150, 180, 210 GPa hydrostaic pressure.

$\varepsilon_2(\omega)$ shows light absorption when a light of suitable frequency falls on it. Threshold values for light absorption are proportional to the optical band gaps,and after these threshold energies, absorption of light starts. This threshold values is 2.8 eV as calculeted from $\varepsilon_2(\omega)$ for K_2TeCl_6. The imaginary dielectric constant $\varepsilon_2(\omega)$ is exhibits positive values at all energy, and overall higher energy shifts with increasing the external pressure. In Figure 5.9, $\varepsilon_2(\omega)$ shows maximum values at 9 eV and then decreses linearly with the increasing pressure.

5.4.2 Absorption Coefficient

Absorption coefficients are the measure of light that might be absorbed by a given thickness of a material. When a substance is exposed to outside light, both transmission and surface reflection are visible. The gradual decay of the impinging intensity when light travels a unit distance in the medium reveals absorption coefficients. The absorption coefficient $\alpha(\omega)$ also describes how much light energy absorbed by semiconductor and sharp absorption edges for theimpinging energy exceeding the bandgap is very important to determine bandgap. The $\alpha(\omega)$ and $\varepsilon_2(\omega)$ both represent absorption of light. In Figure 5.10, At ambient pressure we can see the

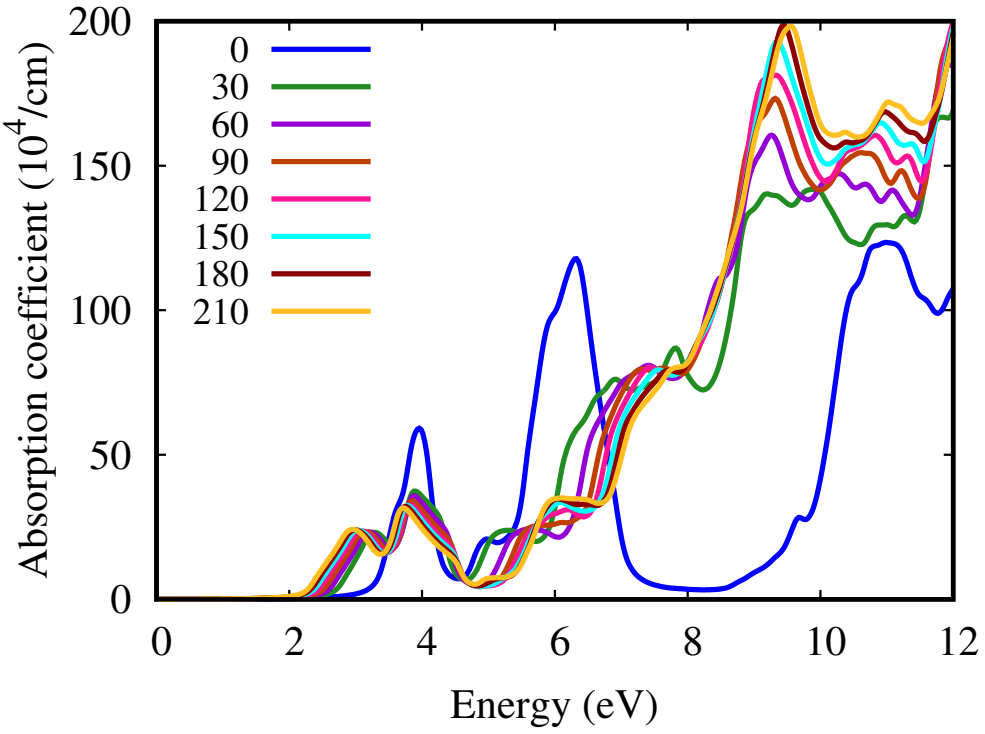

Figure 5.10: Absorption coefficient of vacancy order double perovskite K_2TeCl_6 under 0, 30, 60, 90, 120, 150, 180, 210 GPa hydrostatic pressure.

absorption coefficient for K_2TeCl_6. The range of photon energies for visible light is 1.63 eV to 3.26 eV. As the incident energy increases,the absorption coefficient increases in the visible region and much larger absorption coefficients are observed in the ultraviolet(UV) region. Increasing pressure at early UV region, of absorption coefficient decreases and after 8 eV absorption increases as the photon energy in-

creases. The diagrams of absorption coefficient under various pressure can be seen in Figure 5.10.

5.4.3 Optical Conductivity

Optical conductivity $\sigma(\omega)$ determines the ability of a medium to initiate a phenomenon of conduction as the electromagnetic radiations try to propagate through it. The optical conductivity $\sigma(\omega)$ illustrates the optical current induced due to the liberated free carries as a result of incident energy. The incident photon energy

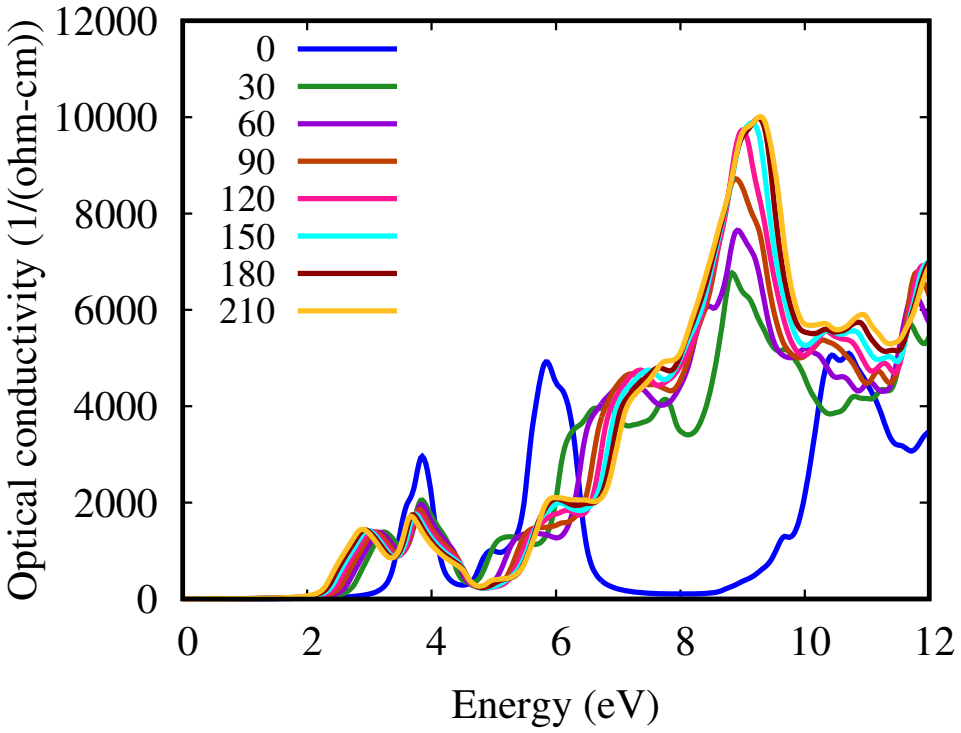

Figure 5.11: Optical conductivity of K_2TeCl_6 halide double perovskite under 0, 30, 60, 90, 120, 150, 180, 210 GPa hydrostatic pressure.

excites bound valence electrons to move to the conduction band. The behavior of optical conductivity and absorption coefficient plots are similar because attenuation of incident light increases electron concentration in the conduction band. The graphical representation of optical conductivity as a function of photon energy illustrates in Figure 5.11 at ambient and under uniform pressure. The peaks of optical conductivity gets sharps with the application of hydrostatic pressure in UV region

(at 9 eV) with applied pressure. The pressure-induced change in band structure is another factor that supports this conclusion.

5.4.4 Optical Reflectivity

Reflectivity is an optical property of material, which describes how much light is reflected from the material with an amount of light incident on the material. A fraction of energy which bounces back from the material medium is calculated as reflectivity $R(\omega)$. The energy dependent $R(\omega)$ dispersion for the studied double perovskite is shown in Figure 5.12. This reflectivity values are associated with real

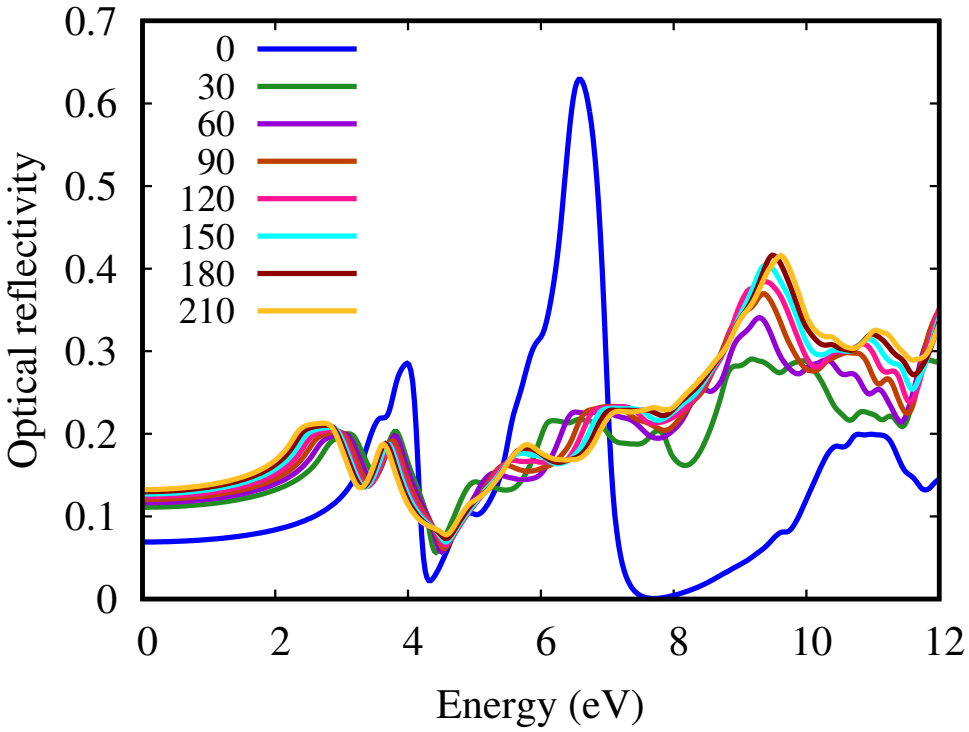

Figure 5.12: Optical reflectivity of K_2TeCl_6 vacancy order double perovskite under 0, 30, 60, 90, 120, 150, 180, 210 GPa hydrostatic pressure.

dielectric constant because highest reflectivity is echibited for the energy values where negative $\varepsilon_1(\omega)$ is exhibited. At ambient pressure, reflectivity starts increasing after the threshold and peak occurs at the boundary of the visible and makes a sharp peak at 6 eV. To investigate deeply the surface behavior of the material, its reflectivity is measured which is equal to the ratio of incident power to reflected power. The reflectivity R(0) computed at zero frequency expand with applied differ-

ent pressure,as illustrated in Figure 5.12. Figure 5.12 shows that the zero frequency limit of reflectivity for K_2TeCl_6 is equal to 0.129, 0.127, 0.128, 0.130, 0.131, 0.132, 0.133 at (30, 60, 90, 120, 150, 180, and 210) GPa respectively. It then increase from its zero limit as with the increase in pressure and reached at the highest peak of reflectivity after 9 eV. Under applied pressure reflectivity increases linearly with the increased photon energy.

5.4.5 Refractive Index

Generally light traversing any material travels slowly as compared to vaccum. This light speed dependence over the density of the material can be evalutated by calculating refractive index. The refractive index $n(\omega)$, that is sensitive to the wavelength, group velocity, and nature of the material, is also computed plotted against energy in Figure 5.13. The change of $n(\omega)$ with respect to the energy is like $\varepsilon_1(\omega)$ and both

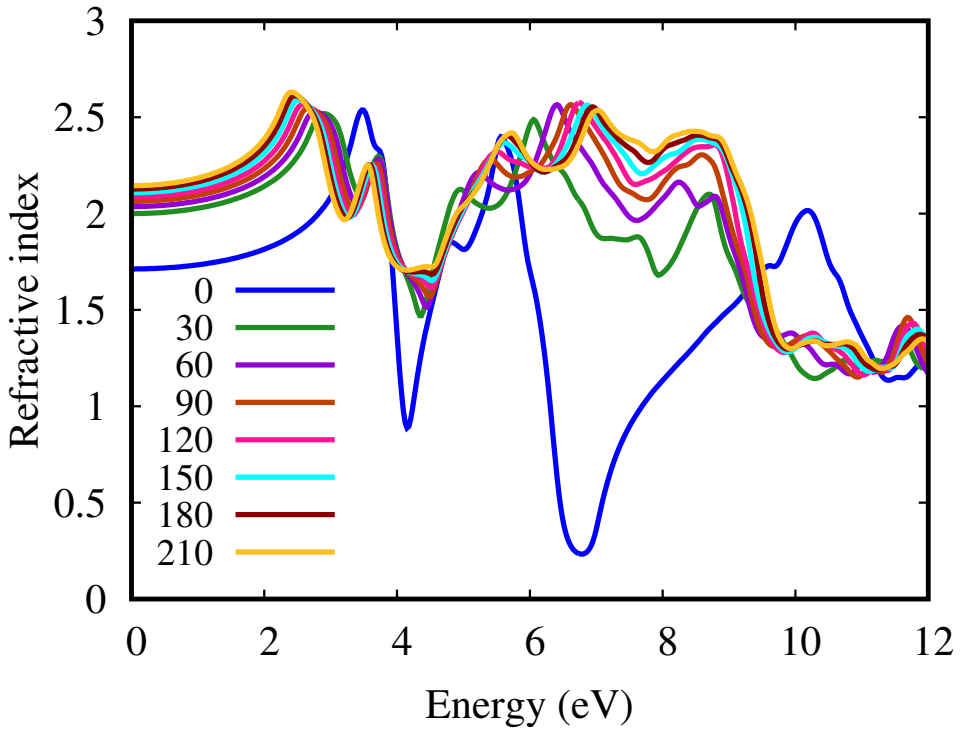

Figure 5.13: Refractive index of vacancy ordered double perovskite K_2TeCl_6 under 0, 30, 60, 90, 120, 150, 180, 210 GPa hydrostatic pressure.

express same information about the material. The relation between static values of real dielectric constant and refractive index ,$n(0) = \varepsilon_1^2(0)$ is satisfied as evidient

from static real dielectric constant. Furthermore, the analysis of $n(\omega)$ in the energy range of 1-3 eV reveals that this compound is important for optical applications due to its unique optical properties in both the infrared and ultraviolet energy ranges. This is attributed to their unique optical properties in both the infrared and ultraviolet energy ranges. The value $n(\omega)$ is 1.73 for K_2TeCl_6 make them more suitable for visible light energy conversion solar cells. The static refractive index n(0) determined at $\omega = 0$ expand with the applied pressure 0, 30, 60, 90, 120, 150, 180, 210 GPa, respectively. The change between the refractive index and photon energy under different pressure has shown in Figure 5.13.

Chapter 6

Conclusion

In this thesis, we investigated the vacancy-ordered double perovskite K_2TeCl_6 for optoelectronic applications using density functional theory as implemented in the WIEN2k code. We explored the structural, mechanical, electrical, and optical properties of K_2TeCl_6 under uniform hydrostatic pressures up to 210 GPa, compared to the ambient conditions.

Our study investigates the material's characteristics under various pressure levels, revealing a reduction in lattice parameter with decreasing volume and bond lengths. Calculated electronic properties depict K_2TeCl_6 as a semiconductor with an indirect band gap, where the lowest energy bands in the conduction region and the highest energy bands in the valence region are located in different symmetry points in the first Brillouin zone. As pressure increases, the band gap decreases from 2.622 eV to 1.797 eV. At ambient pressure, Cl significantly contributes to the valence band, while Tl dominates the conduction band. At ambient condition, analysis of mechanical properties shows that the material exhibits ductile nature, with Poisson's ratio and Pugh's ratio greater than 0.26 and 1.75 respectively. Furthermore, the compound becomes more ductile and stable under hydrostatic pressure compared to ambient condition, making it suitable for pressure sensing applications in industrial and automotive systems.

Conclusion

Optical characteristics undergo alterations in response to pressure variation, with the maximum absorption region spanning from visible to ultraviolet, suggesting suitability for solar cells and other optoelectronic applications. These responsive optical characteristics, particularly the broad absorption region, make K_2TeCl_6 suitable for optoelectronic applications such as photodetectors, LEDs, and solar cells, indicating its potential for practical device application.

In summary, with semiconducting nature and tunable electronic properties under different hydrostatic pressures, K_2TeCl_6 could be a promising candidate for optoelectronic applications.

Bibliography

[1] Priyanka Verma, Yasutaka Kuwahara, Kohsuke Mori, Robert Raja, and Hiromi Yamashita. New insights in establishing the structure-property relations of novel plasmonic nanostructures for clean energy applications. *Energy chem*, 4(1):100070, 2022.

[2] Ashwini K Nangia and Gautam R Desiraju. Crystal engineering: an outlook for the future. *Angewandte chemie international edition*, 58(13):4100–4107, 2019.

[3] DFT study on the crystal structure, optoelectronic, and thermoelectric properties of lead-free inorganic A_2PdBr_6(A= K, Rb, and Cs) perovskites, author=Bousahla, Mohammed Alaa and Faizan, Muhammad and Seddik, Taieb and Omran, Saad Bin and Khachai, Houari and Laref, Amel and Khenata, Rabah and Znaidia, Sami and Boukhris, Imed and Khan, Shah Haidar, journal=Materials today communications, volume=30, pages=103061, year=2022, publisher=Elsevier.

[4] Abeer A AlObaid, Syed Awais Rouf, Tahani I Al-Muhimeed, AI Aljameel, S Bouzgarrou, HH Hegazy, Thamraa Alshahrani, Ghazanfar Nazir, Abeer Mera, and Q Mahmood. New lead-free double perovskites $Rb_2Ge(Cl/Br)_6$; a promising materials for renewable energy applications. *Materials chemistry and physics*, 271:124876, 2021.

[5] Mohammed Alaa Bousahla, Muhammad Faizan, Taieb Seddik, Saad Bin Omran, Houari Khachai, Amel Laref, Rabah Khenata, Sami Znaidia, Imed

Boukhris, and Shah Haidar Khan. Dft study on the crystal structure, optoelectronic, and thermoelectric properties of lead-free inorganic A_2PdBr_6 (A= K, Rb, and Cs) perovskites. *Materials today communications*, 30.

[6] NA Noor, M Waqas Iqbal, Taharh Zelai, Asif Mahmood, HM Shaikh, Shahid M Ramay, and Waheed Al-Masry. Analysis of direct band gap A_2ScInI_6 A= Rb, Cs double perovskite halides using dft approach for renewable energy devices. *Journal of materials research and technology*, 13:2491–2500, 2021.

[7] Ping Hou, Wenxiang Yang, Ning Wan, Zhi Fang, Jinju Zheng, Minghui Shang, Dingfa Fu, Zuobao Yang, and Weiyou Yang. Precursor engineering for high-quality $Cs_2AgBiBr_6$ films toward efficient lead-free double perovskite solar cells. *Journal of materials chemistry*, 9(30):9659–9669, 2021.

[8] Fatima Aslam, B Sabir, and M Hassan. Structural, electronic, optical, thermoelectric, and transport properties of indium-based double perovskite halides Cs_2InAgX_6 (X= Cl, Br, I) for energy applications. *Applied physics A*, 127:1–12, 2021.

[9] David O Obada, Shittu B Akinpelu, Simeon A Abolade, Emmanuel Okafor, Aniekan M Ukpong, Syam Kumar R, and Akinlolu Akande. Lead-free double perovskites: A review of the structural, optoelectronic, mechanical, and thermoelectric properties derived from first-principles calculations, and materials design applicable for pedagogical purposes. *Crystals*, 14(1):86, 2024.

[10] Electronic, optical, and thermoelectric properties of vacancy-ordered double perovskite K_2SnX_6(X= Cl, Br, I) from first-principle calculations, author=Zikem, A and Baaziz, H and Ghellab, T and Charifi, Z and Soyalp, F, journal=Physica scripta, volume=99, number=3, pages=035917, year=2024, publisher=IOP Publishing.

[11] Marcela A Bavio, Julia E Tasca, Gerardo G Acosta, Marcelo F Ponce, Rodolfo O Fuentes, and Arnaldo Visintin. Study of double perovskite La_2B (ii) MnO_6 (B: Ni, Co, Cu) as electrode materials for energy storage. *Journal of solid state electrochemistry*, 24(3):699–710, 2020.

[12] Abhishek Swarnkar, Ashley R Marshall, Erin M Sanehira, Boris D Chernomordik, David T Moore, Jeffrey A Christians, Tamoghna Chakrabarti, and Joseph M Luther. Quantum dot–induced phase stabilization of α-$CsPbI_3$ perovskite for high-efficiency photovoltaics. *Science*, 354(6308):92–95, 2016.

[13] Li Na Quan, Joohoon Kang, Cun-Zheng Ning, and Peidong Yang. Nanowires for photonics. *Chemical reviews*, 119(15):9153–9169, 2019.

[14] Asif Mahmood, NA Noor, M Waqas Iqbal, Ateyah A Al-Zahrani, Young-Han Shin, and Tausif Zahid. Exploration of new double perovskites Cs_2YInX_6 (X= Cl, Br, I) for opto-electronic and sustainable energy applications. *Electrochemical society journal of solid state science and technology*, 10(8):084007, 2021.

[15] Pakeeza Aymen Nawaz, Ghulam M Mustafa, Sadia Sagar Iqbal, NA Noor, Tasawer Shahzad Ahmad, Asif Mahmood, and R Neffati. Theoretical investigations of optoelectronic and transport properties of Rb_2YInX_6 (X= Cl, Br, I) double perovskite materials for solar cell applications. *Solar energy*, 231:586–592, 2022.

[16] Annalise E Maughan, Alex M Ganose, Mitchell M Bordelon, Elisa M Miller, David O Scanlon, and James R Neilson. Defect tolerance to intolerance in the vacancy-ordered double perovskite semiconductors Cs_2SnI_6 and Cs_2TeI_6. *Journal of the American chemical society*, 138(27):8453–8464, 2016.

[17] Byunghong Lee, Constantinos C Stoumpos, Nanjia Zhou, Feng Hao, Christos Malliakas, Chen-Yu Yeh, Tobin J Marks, Mercouri G Kanatzidis, and Robert PH Chang. Air-stable molecular semiconducting iodosalts for solar cell applications: Cs_2SnI_6 as a hole conductor. *Journal of the American chemical society*, 136(43):15379–15385, 2014.

[18] Bayrammurad Saparov, Jon-Paul Sun, Weiwei Meng, Zewen Xiao, Hsin-Sheng Duan, Oki Gunawan, Donghyeop Shin, Ian G Hill, Yanfa Yan, and David B Mitzi. Thin-film deposition and characterization of a sn-deficient perovskite derivative Cs_2SnI_6. *Chemistry of materials*, 28(7):2315–2322, 2016.

[19] T Ghrib, A Rached, Eman Algrafy, Ibtessam A Al-nauim, Hind Albalawi, MGB Ashiq, Bakhtiar Ul Haq, and QJMC Mahmood. A new lead free double perovskites $K_2Ti(Cl/Br)_6$; a promising materials for optoelectronic and transport properties; probed by dft. *Materials chemistry and physics*, 264:124435, 2021.

[20] Annalise E Maughan, Alex M Ganose, Mitchell M Bordelon, Elisa M Miller, David O Scanlon, and James R Neilson. Defect tolerance to intolerance in the vacancy-ordered double perovskite semiconductors Cs_2SnI_6 and Cs_2TeI_6. *Journal of the American chemical society*, 138(27):8453–8464, 2016.

[21] Byunghong Lee, Constantinos C Stoumpos, Nanjia Zhou, Feng Hao, Christos Malliakas, Chen-Yu Yeh, Tobin J Marks, Mercouri G Kanatzidis, and Robert PH Chang. Air-stable molecular semiconducting iodosalts for solar cell applications: Cs_2SnI_6 as a hole conductor. *Journal of the American chemical society*, 136(43):15379–15385, 2014.

[22] Bayrammurad Saparov, Feng Hong, Jon-Paul Sun, Hsin-Sheng Duan, Weiwei Meng, Samuel Cameron, Ian G Hill, Yanfa Yan, and David B Mitzi. Thin-film preparation and characterization of $Cs_3Sb_2I_9$: a lead-free layered perovskite semiconductor. *Chemistry of materials*, 27(16):5622–5632, 2015.

[23] Nobuya Sakai, Amir Abbas Haghighirad, Marina R Filip, Pabitra K Nayak, Simantini Nayak, Alexandra Ramadan, Zhiping Wang, Feliciano Giustino, and Henry J Snaith. Solution-processed cesium hexabromopalladate (iv), Cs_2PdBr_6, for optoelectronic applications. *Journal of the American chemical society*, 139(17):6030–6033, 2017.

[24] Xiaofeng Qiu, Bingqiang Cao, Shuai Yuan, Xiangfeng Chen, Zhiwen Qiu, Yanan Jiang, Qian Ye, Hongqiang Wang, Haibo Zeng, Jian Liu, et al. From unstable $CsSnI_3$ to air-stable Cs_2SnI_6: A lead-free perovskite solar cell light absorber with bandgap of 1.48 ev and high absorption coefficient. *Solar energy materials and solar cells*, 159:227–234, 2017.

[25] Annalise E Maughan, Alex M Ganose, Mitchell M Bordelon, Elisa M Miller, David O Scanlon, and James R Neilson. Defect tolerance to intolerance in the vacancy-ordered double perovskite semiconductors Cs_2SnI_6 and Cs_2TeI_6. *Journal of the American chemical society*, 138(27):8453–8464, 2016.

[26] Yao Cai, Wei Xie, Hong Ding, Yan Chen, Krishnamoorthy Thirumal, Lydia H Wong, Nripan Mathews, Subodh G Mhaisalkar, Matthew Sherburne, and Mark Asta. Computational study of halide perovskite-derived A_2BX_6 inorganic compounds: chemical trends in electronic structure and structural stability. *Chemistry of materials*, 29(18):7740–7749, 2017.

[27] Wan-Jian Yin, Ji-Hui Yang, Joongoo Kang, Yanfa Yan, and Su-Huai Wei. Halide perovskite materials for solar cells: a theoretical review. *Journal of materials chemistry A*, 3(17):8926–8942, 2015.

[28] Lyubov A Frolova, Denis V Anokhin, Kirill L Gerasimov, Nadezhda N Dremova, and Pavel A Troshin. Exploring the effects of the Pb2+ substitution in $MAPbI_3$ on the photovoltaic performance of the hybrid perovskite solar cells. *The journal of physical chemistry letters*, 7(21):4353–4357, 2016.

[29] Nakita K Noel, Samuel D Stranks, Antonio Abate, Christian Wehrenfennig, Simone Guarnera, Amir-Abbas Haghighirad, Aditya Sadhanala, Giles E Eperon, Sandeep K Pathak, Michael B Johnston, et al. Lead-free organic–inorganic tin halide perovskites for photovoltaic applications. *Energy & Environmental science*, 7(9):3061–3068, 2014.

[30] Adam H Slavney, Te Hu, Aaron M Lindenberg, and Hemamala I Karunadasa. A bismuth-halide double perovskite with long carrier recombination lifetime for photovoltaic applications. *Journal of the American chemical society*, 138(7):2138–2141, 2016.

[31] Dianxing Ju, Xiaopeng Zheng, Jun Yin, Zhiwen Qiu, Bekir Türedi, Xiaolong Liu, Yangyang Dang, Bingqiang Cao, Omar F. Mohammed, Osman M. Bakr, and Xutang Tao. Tellurium-based double perovskites A_2TeX_6 with tun-

able band gap and long carrier diffusion length for optoelectronic applications. *American chemical society Energy Letters*, 4(1):228–234, 2019.

[32] Indira Kopacic, Bastian Friesenbichler, Sebastian F Hoefler, Birgit Kunert, Harald Plank, Thomas Rath, and Gregor Trimmel. Enhanced performance of germanium halide perovskite solar cells through compositional engineering. *American chemical society applied energy materials*, 1(2):343–347, 2018.

[33] Mutalifu Abulikemu, Samy Ould-Chikh, Xiaohe Miao, Erkki Alarousu, Banavoth Murali, Guy Olivier Ngongang Ndjawa, Jérémy Barbé, Abdulrahman El Labban, Aram Amassian, and Silvano Del Gobbo. Optoelectronic and photovoltaic properties of the air-stable organohalide semiconductor $(CH_3NH_3)_3Bi_2I_9$. *Journal of materials chemistry A*, 4(32):12504–12515, 2016.

[34] George Volonakis, Marina R. Filip, Amir Abbas Haghighirad, Nobuya Sakai, Bernard Wenger, Henry J. Snaith, and Feliciano Giustino. Lead-free halide double perovskites via heterovalent substitution of noble metals. *The Journal of physical chemistry letters*, 7(7):1254–1259, 2016. PMID: 26982118.

[35] Min Chen, Ming-Gang Ju, Alexander D Carl, Yingxia Zong, Ronald L Grimm, Jiajun Gu, Xiao Cheng Zeng, Yuanyuan Zhou, and Nitin P Padture. Cesium titanium (iv) bromide thin films based stable lead-free perovskite solar cells. *Joule*, 2(3):558–570, 2018.

[36] Ming-Gang Ju, Min Chen, Yuanyuan Zhou, Hector F Garces, Jun Dai, Liang Ma, Nitin P Padture, and Xiao Cheng Zeng. Earth-abundant nontoxic titanium (iv)-based vacancy-ordered double perovskite halides with tunable 1.0 to 1.8 ev bandgaps for photovoltaic applications. *American chemical society energy letters*, 3(2):297–304, 2018.

[37] Ming-Gang Ju, Min Chen, Yuanyuan Zhou, Hector F Garces, Jun Dai, Liang Ma, Nitin P Padture, and Xiao Cheng Zeng. Earth-abundant nontoxic titanium (iv)-based vacancy-ordered double perovskite halides with tunable 1.0 to 1.8 ev bandgaps for photovoltaic applications. *American chemical society energy letters*, 3(2):297–304, 2018.

[38] Kunal Chakraborty, Mahua Gupta Choudhury, and Samrat Paul. Numerical study of Cs_2TiX_6 (X= Br-, I-, F- and Cl-)based perovskite solar cell using scaps-1d device simulation. *Solar energy*, 194:886–892, 2019.

[39] Julie Euvrard, Xiaoming Wang, Tianyang Li, Yanfa Yan, and David B Mitzi. Is Cs_2TiBr_6 a promising pb-free perovskite for solar energy applications? *Journal of materials chemistry A*, 8(7):4049–4054, 2020.

[40] Deying Kong, Dali Cheng, Xuewen Wang, Kaiyuan Zhang, Huachun Wang, Kai Liu, Huanglong Li, Xing Sheng, and Lan Yin. Solution processed lead-free cesium titanium halide perovskites and their structural, thermal and optical characteristics. *Journal of materials chemistry C*, 8(5):1591–1597, 2020.

[41] RO Jones, O Gunnarson, RG Parr, and W Yang. Density-functional theory of atoms and molecules. 1989.

[42] Karlheinz Schwarz and Peter Blaha. Solid state calculations using wien2k. *Computational materials science*, 28:259–273, 10 2003.

[43] Reyhaneh Ebrahimi, Ali Mokhtari, and Vishtasb Soleimanian. Electronic, structural, and magnetic properties of the double perovskite Ba_2MnMoO_6 in different phases using hubbard model. *Journal of superconductivity and novel magnetism*, 29, 05 2016.

[44] S. Haid, W. Benstaali, A. Abbad, B. Bouadjemi, S. Bentata, and Z. Aziz. Thermoelectric, structural, optoelectronic and magnetic properties of double perovskite Sr_2CrTaO_6: First principle study. *Materials science and engineering: B*, 245:68–74, 2019.

[45] K Schwarz. Cro_2 predicted as a half-metallic ferromagnet. *Journal of physics F: metal physics*, 16(9):L211, sep 1986.

[46] C.Q. Tang, Y. Zhang, and J. Dai. Electronic and magnetic structure studies of double perovskite Sr_2CrReO_6 by first-principles calculations. *Solid state communications*, 133(4):219–222, 2005.

[47] R.M. Martin. *Electronic Structure: Basic Theory and Practical Methods*. Cambridge university press, 2004.

[48] E. Schrödinger. An undulatory theory of the mechanics of atoms and molecules. *Phys. Rev.*, 28:1049–1070, Dec 1926.

[49] T Britannica. Editors of encyclopaedia. *Argon. Encyclopedia britannica*, 2020.

[50] David J Griffiths and Darrell F Schroeter. *Introduction to quantum mechanics*. Cambridge university press, 2018.

[51] Max Born. Quantum mechanics of collision processes. *Uspekhi Fizich*, 1926.

[52] Wolfram Koch and Max C Holthausen. The quest for approximate exchangecorrelation functionals. *A chemist's guide to density functional theory*, 65, 2000.

[53] Wolfgang Pauli. The connection between spin and statistics. *Physical Review*, 58(8):716, 1940.

[54] Arthur Jabs. Connecting spin and statistics in quantum mechanics. *Foundations of physics*, 40:776–792, 2010.

[55] Attila Szabo and Neil S Ostlund. *Modern quantum chemistry: introduction to advanced electronic structure theory*. Courier corporation, 2012.

[56] Wolfgang Pauli. On the connexion between the completion of electron groups in an atom with the complex structure of spectra. *Zeitschrift für Physik*, 31:765, 1925.

[57] Nouredine Zettili. Quantum mechanics: concepts and applications, 2003.

[58] Klaus Capelle. A bird's-eye view of density-functional theory. *Brazilian journal of physics*, 36:1318–1343, 2006.

[59] Donald Allan McQuarrie and John Douglas Simon. *Physical chemistry: a molecular approach*, volume 1. university science books sausalito, CA, 1997.

[60] Wolfram Koch and Max C Holthausen. The quest for approximate exchangecorrelation functionals. *A chemist's guide to density functional theory*, 65, 2000.

[61] Max Born and W Heisenberg. Zur quantentheorie der molekeln. *Original scientific papers wissenschaftliche originalarbeiten*, pages 216–246, 1985.

[62] M. Born and R. Oppenheimer. Zur quantentheorie der molekeln. *Annalen der Physik*, 389(20):457–484, 1927. PDF of an english translation by S.M. Blinder is available.

[63] M.P. Marder. *Condensed matter physics*. Wiley, 2010.

[64] Torsten Fließbach and Torsten Fließbach. Streuung. *Mechanik: Lehrbuch zur Theoretischen Physik I*, pages 151–163, 2009.

[65] Franz Schwabl. *Quantenmechanik (QM I): Eine Einführung*. Springer-Verlag, 2007.

[66] Paul Adrien Maurice Dirac. A new notation for quantum mechanics. In *Mathematical proceedings of the cambridge philosophical society*, volume 35, pages 416–418. Cambridge university press, 1939.

[67] David J Griffiths and Darrell F Schroeter. *Introduction to quantum mechanics*. Cambridge university press, 2018.

[68] C. Lang and N. Pucker. *Mathematische Methoden in der Physik*. Springer Berlin Heidelberg, 2005.

[69] A. Szabo, A. Szabó, and N.S. Ostlund. *Modern Quantum Chemistry: Introduction to Advanced Electronic Structure Theory*. Macmillan, 1982.

[70] Eva Pavarini, Erik Koch, and Ulrich Schollwöck. *Emergent Phenomena in Correlated Matter: Lecture Notes of the Autumn School Correlated Electrons 2013, at Forschungszentrum Jülich, 23-27 September 2013*, volume 3. Forschungszentrum Jülich, 2013.

[71] Walter Kohn. Nobel lecture: Electronic structure of matter—wave functions and density functionals. *Reviews of modern physics*, 71(5):1253, 1999.

[72] Björn O Roos. *Lecture notes in quantum chemistry*, volume 58. Springer, 1992.

[73] NM Harrison. An introduction to density functional theory. *Nato Science Series Sub Series III Computer and Systems Sciences*, 187:45–70, 2003.

[74] Frank Jensen. *Introduction to computational chemistry*. John wiley & sons, 2017.

[75] Zhiping Yin. *Microscopic mechanisms of magnetism and superconductivity studied from first principle calculations*. University of california, Davis, 2009.

[76] Pierre Hohenberg and Walter Kohn. Inhomogeneous electron gas. *Physical review*, 136(3B):B864, 1964.

[77] LH Thomas. Proc. cambridge philos. *Soc*, 23:542, 1927.

[78] Enrico Fermi. Eine statistische methode zur bestimmung einiger eigenschaften des atoms und ihre anwendung auf die theorie des periodischen systems der elemente. *Zeitschrift für Physik*, 48(1-2):73–79, 1928.

[79] Robert O Jones and Olle Gunnarsson. The density functional formalism, its applications and prospects. *Reviews of modern physics*, 61(3):689, 1989.

[80] Edward Teller. On the stability of molecules in the thomas-fermi theory. *Reviews of modern physics*, 34(4):627, 1962.

[81] Nandor L Balàzs. Formation of stable molecules within the statistical theory of atoms. *Physical review*, 156(1):42, 1967.

[82] Walter Kohn and Lu Jeu Sham. Self-consistent equations including exchange and correlation effects. *Physical review*, 140(4A):A1133, 1965.

[83] J Pierre, RV Skolozdra, J Tobola, S Kaprzyk, C Hordequin, MA Kouacou, I Karla, R Currat, and E Lelievre-Berna. Properties on request in semi-heusler phases. *Journal of alloys and compounds*, 262:101–107, 1997.

[84] Jan Adriaan Berger. *Current-density functionals in extended systems*. University library groningen][Host], 2006.

[85] Walter Kohn. Density functional theory: Basic results and some observations. *Density functional methods in physics*, pages 1–9, 1985.

[86] Juan Carlos Cuevas. Introduction to density functional theory. *Universität Karlsruhe, Germany*, 2010.

[87] Klaus Capelle. A bird's-eye view of density-functional theory. *Brazilian journal of physics*, 36:1318–1343, 2006.

[88] Mel Levy. Universal variational functionals of electron densities, first-order density matrices, and natural spin-orbitals and solution of the v-representability problem. *Proceedings of the national cademy of sciences*, 76(12):6062–6065, 1979.

[89] Elliott H Lieb. Density functionals for coulomb systems. *Inequalities: Selecta of Elliott H. Lieb*, pages 269–303, 2002.

[90] Swapan K Ghosh. Energy derivatives in density-functional theory. *Chemical physics letters*, 172(1):77–82, 1990.

[91] Eugene S Kryachko and Eduardo V Ludeña. *Energy density functional theory of many-electron systems*, volume 4. Springer Science & Business Media, 2012.

[92] Zenebe Assefa Tsegaye. Density functional theory studies of electronic and optical properties of ZnS alloyed with mn and cr. Master's thesis, Institutt for fysikk, 2012.

[93] L Mehdaoui, R Miloua, M Khadraoui, MO Bensaid, D Abdelkader, F Chiker, and A Bouzidi. Theoretical analysis of electronic, optical, photovoltaic and thermoelectric properties of $AgBiS_2$. *Physica B: condensed matter*, 564:114–124, 2019.

[94] Yao Cai, Wei Xie, Hong Ding, Yan Chen, Krishnamoorthy Thirumal, Lydia H Wong, Nripan Mathews, Subodh G Mhaisalkar, Matthew Sherburne,

and Mark Asta. Computational study of halide perovskite-derived A_2BX_6 inorganic compounds: chemical trends in electronic structure and structural stability. *Chemistry of materials*, 29(18):7740–7749, 2017.

[95] Murugesan Rasukkannu, Dhayalan Velauthapillai, and Ponniah Vajeeston. A first-principle study of the electronic, mechanical and optical properties of inorganic perovskite Cs_2SnI_6 for intermediate-band solar cells. *Materials letters*, 218:233–236, 2018.

[96] Yuanyuan Kong, Yonghua Duan, Lishi Ma, and Runyue Li. Phase stability, elastic anisotropy and electronic structure of cubic MAl_2 (M= Mg, Ca, Sr and Ba) laves phases from first-principles calculations. *Materials research express*, 3(10):106505, 2016.

[97] E Deligoz and H Ozisik. Mechanical and dynamical stability of TiAsTe compound from ab initio calculations. *Philosophical magazine*, 95(21):2294–2305, 2015.

[98] Aneeza Iftikhar, Afaq Ahmad, Iftikhar Ahmad, and Muhammad Rizwan. Dft study on thermo-elastic properties of Ru_2FeZ (Z= Si, Ge, Sn) heusler alloys. *International journal of modern physics B*, 32(05):1850045, 2018.

[99] R Hill. First-principles elastic constants for the hcp transition metals fe, co, and re at high pressure. In *Proc. Phys. Soc*, volume 65, page 350, 1952.

[100] SF Pugh. Xcii. relations between the elastic moduli and the plastic properties of polycrystalline pure metals. *The London, Edinburgh, and Dublin Philosophical Magazine and Journal of Science*, 45(367):823–843, 1954.

[101] NA Noor, W Tahir, Fatima Aslam, and A Shaukat. Ab initio study of structural, electronic and optical properties of Be-doped CdS, CdSe and CdTe compounds. *Physica B: condensed matter*, 407(6):943–952, 2012.

[102] Alexander E Fedorovskiy, Nikita A Drigo, and Mohammad Khaja Nazeeruddin. The role of goldschmidt's tolerance factor in the formation of A_2BX_6

double halide perovskites and its optimal range. *Small methods*, 4(5):1900426, 2020.

[103] GV Sin'Ko and NA Smirnov. Ab initio calculations of elastic constants and thermodynamic properties of bcc, fcc, and hcp al crystals under pressure. *Journal of physics: condensed matter*, 14(29):6989, 2002.

[104] Lalhriatpuia Hnamte, Sandeep Sandeep, Himanshu Joshi, and RK Thapa. Electronic and optical properties of double perovskite Ba_2VMoO_6: Fp-lapw study. In *American institute of physics conference proceedings*, volume 1953. American institute of physics publishing, 2018.

[105] Yao Cai, Wei Xie, Yin Ting Teng, Padinhare Cholakkal Harikesh, Biplab Ghosh, Patrick Huck, Kristin A Persson, Nripan Mathews, Subodh G Mhaisalkar, Matthew Sherburne, et al. High-throughput computational study of halide double perovskite inorganic compounds. *Chemistry of materials*, 31(15):5392–5401, 2019.

[106] David R Penn. Wave-number-dependent dielectric function of semiconductors. *Physical review*, 128(5):2093, 1962.

[107] F Tran. Wien2k: An augmented plane wave plus local orbitals program for calculating crystal properties. 2018.